
Improving Diffusion Models for Inverse Problems Using Optimal Posterior Covariance

Xinyu Peng¹ Ziyang Zheng¹ Wenrui Dai¹ Nuoqian Xiao¹ Chenglin Li¹ Junni Zou¹ Hongkai Xiong¹

Abstract

Recent diffusion models provide a promising zero-shot solution to noisy linear inverse problems without retraining for specific inverse problems. In this paper, we propose the first unified interpretation for existing zero-shot methods from the perspective of approximating the conditional posterior mean for the reverse diffusion process of conditional sampling. We reveal that recent methods are equivalent to making isotropic Gaussian approximations to intractable posterior distributions over clean images given diffused noisy images, with the only difference in the handcrafted design of isotropic posterior covariances. Inspired by this finding, we propose a general plug-and-play posterior covariance optimization based on maximum likelihood estimation to improve recent methods. To achieve optimal posterior covariance without retraining, we provide general solutions based on two approaches specifically designed to leverage pre-trained models with and without reverse covariances. Experimental results demonstrate that the proposed methods significantly enhance the overall performance or robustness to hyperparameters of recent methods. Code is available at <https://github.com/xypeng9903/k-diffusion-inverse-problems>

1. Introduction

Noisy linear inverse problems are widely studied for a variety of image processing tasks, including denoising, inpainting, deblurring, and super-resolution. The noisy linear inverse problems are formulated to accommodate the widely adopted degradation model where images are measured with a linear projection under noise corruption.

¹School of Electronic Information and Electrical Engineering, Shanghai Jiao Tong University, Shanghai 200240, China. Correspondence to: Xinyu Peng <xypeng9903@sjtu.edu.cn>, Wenrui Dai <daiwenrui@sjtu.edu.cn>.

Recently, diffusion models have been emerging as promising methods for solving inverse problems. According to the training strategies, these methods can be categorized into two groups: 1) *supervised methods* that aim to learn a conditional diffusion model using datasets consisting of pairs of degraded and clean images (Saharia et al., 2022; Whang et al., 2022; Luo et al., 2023; Chan et al., 2023), and 2) *zero-shot methods* that leverage pre-trained unconditional diffusion models for conditional sampling in various scenarios of inverse problems without the requirement of retraining. In this paper, we focus on the zero-shot methods that can accommodate various tasks without retraining. To ensure the consistency of optimizing fidelity under conditional sampling, existing zero-shot methods adopt projection onto the measurement subspace (Choi et al., 2021; Lugmayr et al., 2022; Song et al., 2022; Wang et al., 2023; Zhu et al., 2023), leverage the similar idea as classifier guidance (Song et al., 2021b; Dhariwal & Nichol, 2021) to modify the sampling process with the likelihood score (Song et al., 2023; Chung et al., 2023), or resort to variational inference (Feng et al., 2023; Mardani et al., 2023).

Diffusion models initially establish a forward process that introduces noise to the original data \mathbf{x}_0 to generate noisy data \mathbf{x}_t at time t , and then implement the reverse process to generate \mathbf{x}_0 obeying the distribution of original data. The key to realize the reverse process is the posterior mean $\mathbb{E}[\mathbf{x}_0|\mathbf{x}_t] = \int \mathbf{x}_0 p_t(\mathbf{x}_0|\mathbf{x}_t) d\mathbf{x}_0$ that could be the optimal estimation of \mathbf{x}_0 given \mathbf{x}_t in the sense of minimum mean square error (MMSE). In the reverse process for conditional sampling in inverse problems, estimating \mathbf{x}_0 is based on both \mathbf{x}_t and measurement \mathbf{y} . Thus, the optimal estimation is determined by the *conditional posterior mean* $\mathbb{E}[\mathbf{x}_0|\mathbf{x}_t, \mathbf{y}]$.

In this paper, we provide the first unified interpretation for zero-shot methods from the view of approximating the conditional posterior mean for the reverse diffusion process of conditional sampling. We interpret recent zero-shot methods (Song et al., 2023; Chung et al., 2023; Wang et al., 2023; Zhu et al., 2023) with two types of guidance that uniformly employ an isotropic Gaussian approximation for the intractable posterior distribution $p_t(\mathbf{x}_0|\mathbf{x}_t)$ to approximate the conditional posterior mean. Motivated by the insight, we reveal their limitation in handcrafted design of posterior

covariance and propose a generalized method for improving recent methods that optimize the posterior covariance based on maximum likelihood estimation. We achieve optimal posterior covariance using pre-trained unconditional diffusion models in a plug-and-play fashion by converting (available) reverse covariances or via Monte Carlo estimation without reverse covariances. Remarkably, this is the first attempt that successfully predicts posterior covariance in addition to posterior mean from a general class of existing unconditional diffusion models. Experimental results demonstrate that the proposed method significantly outperforms existing zero-shot methods in a wide range of tasks like inpainting, deblurring, and super-resolution, and enhances the robustness to hyperparameters.

2. Background

2.1. Bayesian Framework for Solving Inverse Problems

In inverse problems, we wish to recover the unknown signal $\mathbf{x}_0 \in \mathbb{R}^d$ from noisy measurements $\mathbf{y} \in \mathbb{R}^m$, where

$$\mathbf{y} = \mathbf{A}\mathbf{x}_0 + \mathbf{n} \quad (1)$$

It is usually assumed that by the expert knowledge of the sensing device, $\mathbf{A} \in \mathbb{R}^{m \times d}$ is known and $\mathbf{n} \sim \mathcal{N}(\mathbf{0}, \sigma^2 \mathbf{I})$ is an i.i.d. additive Gaussian noise with a known standard deviation of σ . However, recovering \mathbf{x}_0 from the degraded measurements \mathbf{y} becomes ill-posed due to the under-determined \mathbf{A} and the existence of noise. To solve the ill-posed inverse problem, a prior is required to constrain the solution according to desired image statistics (Feng et al., 2023). From a Bayesian perspective, the prior is described by assuming \mathbf{x}_0 obeys an unknown prior distribution $p(\mathbf{x}_0)$, and we have a likelihood function $p(\mathbf{y}|\mathbf{x}_0) = \mathcal{N}(\mathbf{y}|\mathbf{A}\mathbf{x}_0, \sigma^2 \mathbf{I})$ determined by equation 1. We solve inverse problems by formulating a posterior distribution $p(\mathbf{x}_0|\mathbf{y})$ over clean images given noisy measurements, which in principle is determined given $p(\mathbf{x}_0)$ and $p(\mathbf{y}|\mathbf{x}_0)$ by Bayes’ theorem: $p(\mathbf{x}_0|\mathbf{y}) = p(\mathbf{x}_0)p(\mathbf{y}|\mathbf{x}_0) / \int p(\mathbf{x}_0)p(\mathbf{y}|\mathbf{x}_0)d\mathbf{x}_0$.

2.2. Diffusion Models and Conditioning

We use diffusion models to model the complex posterior distribution $p(\mathbf{x}_0|\mathbf{y})$ for inverse problems. Let us define a family of Gaussian perturbation kernels $p_t(\mathbf{x}_t|\mathbf{x}_0)$ of $\mathbf{x}_0 \sim p(\mathbf{x}_0)$ by injecting *i.i.d.* Gaussian noise of standard deviation σ_t to \mathbf{x}_0 and scaling by the factor of s_t , *i.e.*, $p_t(\mathbf{x}_t|\mathbf{x}_0) = \mathcal{N}(\mathbf{x}_t|s_t\mathbf{x}_0, s_t^2\sigma_t^2\mathbf{I})$, where σ_t is monotonically increasing with respect to time $t = 0, 1, \dots, T$. We start from $\sigma_0 = 0$ and reach a value of σ_T that is much larger than the standard deviation of $p(\mathbf{x}_0)$, to ensure that samples from $\mathbf{x}_T \sim p(\mathbf{x}_T)$ are indistinguishable to samples from $\mathcal{N}(\mathbf{0}, s_T^2\sigma_T^2\mathbf{I})$. Since \mathbf{x}_t is independent of \mathbf{y} once \mathbf{x}_0 is known, we characterize the joint distribution between

\mathbf{x}_0 , \mathbf{y} , and \mathbf{x}_t as $p_t(\mathbf{x}_0, \mathbf{y}, \mathbf{x}_t) = p(\mathbf{x}_0)p(\mathbf{y}|\mathbf{x}_0)p_t(\mathbf{x}_t|\mathbf{x}_0)$, which can also be represented by a probabilistic graphical model $\mathbf{y} \leftarrow \mathbf{x}_0 \rightarrow \mathbf{x}_t$. There exist multiple formulations of diffusion models in the literature (Song & Ermon, 2019; Ho et al., 2020; Song et al., 2021a; Kingma et al., 2021; Song et al., 2021b; Karras et al., 2022). Here, we use the ordinary differential equation (ODE) formulation and select $s_t = 1, \sigma_t = t$ as suggested in (Karras et al., 2022) for simplicity. Let us consider the following ODE:

$$d\mathbf{x}_t = \frac{\mathbf{x}_t - \mathbb{E}[\mathbf{x}_0|\mathbf{x}_t]}{t}dt, \quad \mathbf{x}_T \sim p_T(\mathbf{x}_T). \quad (2)$$

In equation 2, the only source of randomness is the initial sample $\mathbf{x}_T \sim p_T(\mathbf{x}_T)$. The ODE possesses an important property that \mathbf{x}_t generated by the ODE maintains the exact same marginals to \mathbf{x}_t obtained by injecting Gaussian noise to \mathbf{x}_0 , *i.e.*, $p_t(\mathbf{x}_t)$. Generally, diffusion models approximate $\mathbb{E}[\mathbf{x}_0|\mathbf{x}_t]$ with a time-dependent denoiser $D_t(\mathbf{x}_t)$ (referred to as the unconditional diffusion model throughout the paper) that is trained by minimizing the L_2 loss for all $t \in [0, T]$:

$$\min_{D_t} \mathbb{E}_{p_t(\mathbf{x}_0, \mathbf{x}_t)} [\|\mathbf{x}_0 - D_t(\mathbf{x}_t)\|_2^2]. \quad (3)$$

With sufficient data and model capacity, the optimal $D_t(\mathbf{x}_t)$ is the MMSE estimator of \mathbf{x}_0 given \mathbf{x}_t and equals to $\mathbb{E}[\mathbf{x}_0|\mathbf{x}_t]$. Thus, samples from $p(\mathbf{x}_0)$ can be obtained by first sampling \mathbf{x}_T from $\mathcal{N}(\mathbf{0}, s_T^2\sigma_T^2\mathbf{I})$ and then simulating equation 2 from $t = T$ to $t = 0$ using black box ODE solver that replaces $\mathbb{E}[\mathbf{x}_0|\mathbf{x}_t]$ with a well-trained $D_t(\mathbf{x}_t)$.

To solve inverse problems, we are interested in $p(\mathbf{x}_0|\mathbf{y})$. We condition the diffusion models and formulate an ODE whose marginals are $p_t(\mathbf{x}_t|\mathbf{y})$ such that we can simulate the ODE to sample from $p(\mathbf{x}_0|\mathbf{y})$. The desired ODE is

$$d\mathbf{x}_t = \frac{\mathbf{x}_t - \mathbb{E}[\mathbf{x}_0|\mathbf{x}_t, \mathbf{y}]}{t}dt, \quad \mathbf{x}_T \sim p_T(\mathbf{x}_T|\mathbf{y}). \quad (4)$$

For sufficiently large σ_T , samples $\mathbf{x}_T \sim p(\mathbf{x}_T|\mathbf{y})$ are indistinguishable to samples from $\mathcal{N}(\mathbf{0}, s_T^2\sigma_T^2\mathbf{I})$ (see Appendix D.2 in (Dhariwal & Nichol, 2021)). The unconditioned sampling procedure in equation 2 can be used to achieve conditioned sampling in equation 4, by substituting $\mathbb{E}[\mathbf{x}_0|\mathbf{x}_t]$ with the conditional posterior mean $\mathbb{E}[\mathbf{x}_0|\mathbf{x}_t, \mathbf{y}]$ ¹.

3. Unified Interpretation of Diffusion-based Solvers to Inverse Problems

To simulate equation 4 for solving inverse problems, a standard approach is training a conditional diffusion model for approximating $\mathbb{E}[\mathbf{x}_0|\mathbf{x}_t, \mathbf{y}]$ using supervised learning. However, this approach can be computationally demanding by

¹Note that this conclusion can be extended to DDPM, DDIM, and SDE-formalized diffusion models.

training separate models for different scenarios. In this paper, we aim to leverage pre-trained unconditional diffusion models for conditional sampling in inverse problems to avoid additional training. We summarize three steps below: 1) Obtain the estimation of $\mathbb{E}[\mathbf{x}_0|\mathbf{x}_t]$ through the unconditional diffusion model $D_t(\mathbf{x}_t)$; 2) Obtain the estimation of the conditional posterior mean $\mathbb{E}[\mathbf{x}_0|\mathbf{x}_t, \mathbf{y}]$ based on the estimation of $\mathbb{E}[\mathbf{x}_0|\mathbf{x}_t]$; 3) Substitute the estimation of $\mathbb{E}[\mathbf{x}_0|\mathbf{x}_t, \mathbf{y}]$ for $\mathbb{E}[\mathbf{x}_0|\mathbf{x}_t]$ in the sampling process (see equation 2 and equation 4).

Recent zero-shot methods, including DPS (Chung et al., 2023), Π GDM (Song et al., 2023), DDNM (Wang et al., 2023), and DiffPIR (Zhu et al., 2023), explicitly or implicitly follow the three steps but only differ in the estimation of $\mathbb{E}[\mathbf{x}_0|\mathbf{x}_t, \mathbf{y}]$ from $\mathbb{E}[\mathbf{x}_0|\mathbf{x}_t]$ in Step 2). Specifically, these methods can be unified with the interpretation of estimating $\mathbb{E}[\mathbf{x}_0|\mathbf{x}_t, \mathbf{y}]$ with isotropic Gaussian approximations $\mathcal{N}(\mathbf{x}_0|\mathbb{E}[\mathbf{x}_0|\mathbf{x}_t], r_t^2\mathbf{I})$ to the intractable posterior $p_t(\mathbf{x}_0|\mathbf{x}_t)$ with different r_t , as summarized in Table 1. We classify them into two categories, *i.e.*, Type I and Type II guidance, according to approximation paradigms, as elaborated below.

3.1. Type I Guidance: Approximating the Likelihood Score Function

We classify DPS and Π GDM into one category, referred to as Type I guidance. Type I guidance is closely related to classifier guidance (Dhariwal & Nichol, 2021), where the conditional posterior mean $\mathbb{E}[\mathbf{x}_0|\mathbf{x}_t, \mathbf{y}]$ is approximated based on the following proposition.

Proposition 1. *The conditional posterior mean equals to the posterior mean drifted by scaled likelihood score function. Formally,*

$$\mathbb{E}[\mathbf{x}_0|\mathbf{x}_t, \mathbf{y}] = \mathbb{E}[\mathbf{x}_0|\mathbf{x}_t] + s_t\sigma_t^2\nabla_{\mathbf{x}_t} \log p_t(\mathbf{y}|\mathbf{x}_t). \quad (5)$$

Proof. Please refer to Appendix A.2. \square

According to Proposition 1², we can approximate $\mathbb{E}[\mathbf{x}_0|\mathbf{x}_t]$ using the pre-trained unconditional diffusion model $D_t(\mathbf{x}_t)$; however, the likelihood score $\nabla_{\mathbf{x}_t} \log p_t(\mathbf{y}|\mathbf{x}_t)$ is computationally intractable. In inverse problems, only the likelihood $p(\mathbf{y}|\mathbf{x}_0)$ at $t = 0$ is known, and $p_t(\mathbf{y}|\mathbf{x}_t)$ for any $t > 0$ is obtained by an intractable integral over all possible \mathbf{x}_0 as

$$p_t(\mathbf{y}|\mathbf{x}_t) = \int p(\mathbf{y}|\mathbf{x}_0)p_t(\mathbf{x}_0|\mathbf{x}_t)d\mathbf{x}_0. \quad (6)$$

Thus, Type I guidance like DPS (Chung et al., 2023) and Π GDM (Song et al., 2023) in nature approximately com-

²In addition to realizing guidance for diffusion models, Proposition 1 can be used for refining the estimation of \mathbf{x}_0 for learning sampling patterns in MRI (Ravula et al., 2023) and realizing guidance for flow-based generative models to solve inverse problems (Pokle et al., 2023).

Methods	Guidance	r_t
DPS (Chung et al., 2023)	I	approach 0
Π GDM (Song et al., 2023)	I	$\sqrt{\sigma_t^2/(\sigma_t^2 + 1)}$
DDNM (Wang et al., 2023)	II	any fixed value
DiffPIR (Zhu et al., 2023)	II	$\sigma_t/\sqrt{\lambda}$

Table 1: **Unified interpretation of diffusion-based solvers to inverse problems.** Recent methods can be regarded as making isotropic Gaussian approximations to the posterior distributions over clean images given noisy images.

putes $p_t(\mathbf{y}|\mathbf{x}_t)$ based on isotropic Gaussian approximations to the true posterior $p_t(\mathbf{x}_0|\mathbf{x}_t)$.

DPS (Chung et al., 2023) DPS can be viewed as approximating $p_t(\mathbf{x}_0|\mathbf{x}_t)$ using a delta distribution $\delta(\mathbf{x}_0 - \mathbb{E}[\mathbf{x}_0|\mathbf{x}_t])$ centered at the posterior mean $\mathbb{E}[\mathbf{x}_0|\mathbf{x}_t]$, which can be regarded as the limit of the Gaussian $\mathcal{N}(\mathbf{x}_0|\mathbb{E}[\mathbf{x}_0|\mathbf{x}_t], r_t^2\mathbf{I})$ when the variance r_t^2 approaches zero. The likelihood $p_t(\mathbf{y}|\mathbf{x}_t)$ is approximated by

$$\begin{aligned} p_t(\mathbf{y}|\mathbf{x}_t) &\approx \int p(\mathbf{y}|\mathbf{x}_0)\delta(\mathbf{x}_0 - \mathbb{E}[\mathbf{x}_0|\mathbf{x}_t])d\mathbf{x}_0 \\ &= p(\mathbf{y}|\mathbf{x}_0 = \mathbb{E}[\mathbf{x}_0|\mathbf{x}_t]). \end{aligned} \quad (7)$$

However, $p(\mathbf{y}|\mathbf{x}_0 = \mathbb{E}[\mathbf{x}_0|\mathbf{x}_t])$ is not a good approximation to compute the likelihood score $\nabla_{\mathbf{x}_t} \log p_t(\mathbf{y}|\mathbf{x}_t)$ in practice (Chung et al., 2023). To address this issue, DPS empirically adjusts the strength of guidance by replacing the likelihood score $\nabla_{\mathbf{x}_t} \log p_t(\mathbf{y}|\mathbf{x}_t)$ with $-\zeta_t\nabla_{\mathbf{x}_t}\|\mathbf{y} - \mathbf{A}\mathbb{E}[\mathbf{x}_0|\mathbf{x}_t]\|_2^2$, where $\zeta_t = \zeta/\|\mathbf{y} - \mathbf{A}\mathbb{E}[\mathbf{x}_0|\mathbf{x}_t]\|$ with a hyper-parameter ζ .

Π GDM (Song et al., 2023) The delta distribution used in DPS is a very rough approximation to $p_t(\mathbf{x}_0|\mathbf{x}_t)$ as it completely ignores the uncertainty of \mathbf{x}_0 given \mathbf{x}_t . As t increases, the uncertainty in $p_t(\mathbf{x}_0|\mathbf{x}_t)$ becomes larger and is close to the original data distribution $p(\mathbf{x}_0)$. Thus, it is more reasonable to choose a positive r_t . In Π GDM, r_t is heuristically selected as $\sqrt{\sigma_t^2/(1 + \sigma_t^2)}$ under the assumption that $p(\mathbf{x}_0)$ is the standard normal distribution $\mathcal{N}(\mathbf{0}, \mathbf{I})$. In such case, the likelihood $p_t(\mathbf{y}|\mathbf{x}_t)$ is approximated by

$$\begin{aligned} p_t(\mathbf{y}|\mathbf{x}_t) &\approx \int \mathcal{N}(\mathbf{y}|\mathbf{A}\mathbf{x}_0, \sigma^2\mathbf{I})\mathcal{N}(\mathbf{x}_0|\mathbb{E}[\mathbf{x}_0|\mathbf{x}_t], r_t^2\mathbf{I})d\mathbf{x}_0 \\ &= \mathcal{N}(\mathbf{y}|\mathbf{A}\mathbb{E}[\mathbf{x}_0|\mathbf{x}_t], \sigma^2\mathbf{I} + r_t^2\mathbf{A}\mathbf{A}^T). \end{aligned} \quad (8)$$

According to equation 8, the likelihood score is a vector-Jacobian product that can be computed using back-propagation (Song et al., 2023).

3.2. Type II Guidance: Approximating the Conditional Posterior Mean Using Proximal Solution

We classify DiffPIR and DDNM into the category of Type II guidance. Type II guidance approximates the conditional

posterior mean $\mathbb{E}[\mathbf{x}_0|\mathbf{x}_t, \mathbf{y}]$ by finding a solution $\hat{\mathbf{x}}_0^{(t)}$ that is close to $\mathbb{E}[\mathbf{x}_0|\mathbf{x}_t]$ and consistent with the measurement \mathbf{y} at the same time. Compared to Type I guidance, Type II guidance is more efficient by circumventing the expensive back-propagation of the unconditional diffusion model $D_t(\mathbf{x}_t)$ for evaluating gradients. Although Type II guidance seems to be developed from a different perspective, we show that it can also be regarded as an isotropic Gaussian approximation to the true posterior $p_t(\mathbf{x}_0|\mathbf{x}_t)$.

DiffPIR (Zhu et al., 2023) The core step in DiffPIR is replacing $\mathbb{E}[\mathbf{x}_0|\mathbf{x}_t]$ in the unconditional sampling process with the solution to the following proximal problem:

$$\hat{\mathbf{x}}_0^{(t)} = \arg \min_{\mathbf{x}_0} \|\mathbf{y} - \mathbf{A}\mathbf{x}_0\|^2 + \rho_t \|\mathbf{x}_0 - \mathbb{E}[\mathbf{x}_0|\mathbf{x}_t]\|^2, \quad (9)$$

where $\rho_t = \lambda\sigma^2/\sigma_t^2$ and λ is a hyper-parameter. Our key insight is that equation 9 for DiffPIR can be interpreted as approximating $\mathbb{E}[\mathbf{x}_0|\mathbf{x}_t, \mathbf{y}]$ with the mean of an approximate distribution $q_t(\mathbf{x}_0|\mathbf{x}_t, \mathbf{y})$ derived from the isotropic Gaussian approximation $q_t(\mathbf{x}_0|\mathbf{x}_t)$ to the intractable posterior distribution $p_t(\mathbf{x}_0|\mathbf{x}_t)$. Let us define the isotropic Gaussian approximation $q_t(\mathbf{x}_0|\mathbf{x}_t) = \mathcal{N}(\mathbf{x}_0|\mathbb{E}[\mathbf{x}_0|\mathbf{x}_t], r_t^2\mathbf{I})$. We can obtain that the approximate distribution $q_t(\mathbf{x}_0|\mathbf{x}_t, \mathbf{y}) \propto p(\mathbf{y}|\mathbf{x}_0)q_t(\mathbf{x}_0|\mathbf{x}_t)$ for $p_t(\mathbf{x}_0|\mathbf{x}_t, \mathbf{y}) \propto p(\mathbf{y}|\mathbf{x}_0)p_t(\mathbf{x}_0|\mathbf{x}_t)$ ³ is also a Gaussian and its mean $\mathbb{E}_q[\mathbf{x}_0|\mathbf{x}_t, \mathbf{y}]$ can be obtained by solving the optimization problem:

$$\begin{aligned} & \mathbb{E}_q[\mathbf{x}_0|\mathbf{x}_t, \mathbf{y}] \\ &= \arg \max_{\mathbf{x}_0} \log q_t(\mathbf{x}_0|\mathbf{x}_t, \mathbf{y}) \\ &= \arg \max_{\mathbf{x}_0} [\log p(\mathbf{y}|\mathbf{x}_0) + \log q_t(\mathbf{x}_0|\mathbf{x}_t)] \\ &= \arg \min_{\mathbf{x}_0} \left[\|\mathbf{y} - \mathbf{A}\mathbf{x}_0\|^2 + \frac{\sigma^2}{r_t^2} \|\mathbf{x}_0 - \mathbb{E}[\mathbf{x}_0|\mathbf{x}_t]\|^2 \right]. \quad (10) \end{aligned}$$

Note that equation 9 used in DiffPIR is a special case of equation 10 with $r_t = \sigma_t/\sqrt{\lambda}$. Therefore, DiffPIR can be viewed as using isotropic Gaussian approximation $q_t(\mathbf{x}_0|\mathbf{x}_t) = \mathcal{N}(\mathbf{x}_0|\mathbb{E}[\mathbf{x}_0|\mathbf{x}_t], (\sigma_t^2/\lambda)\mathbf{I})$ for $p_t(\mathbf{x}_0|\mathbf{x}_t)$.

DDNM (Wang et al., 2023) The core step in DDNM resorts to the range-null space decomposition of $\mathbb{E}[\mathbf{x}_0|\mathbf{x}_t]$. Specifically, to ensure the measurement consistency $\mathbf{y} = \mathbf{A}\hat{\mathbf{x}}_0^{(t)}$ of the solution $\hat{\mathbf{x}}_0^{(t)}$, DDNM formulates $\hat{\mathbf{x}}_0^{(t)} = \mathbf{A}^\dagger\mathbf{y} + (\mathbf{I} - \mathbf{A}^\dagger\mathbf{A})\mathbb{E}[\mathbf{x}_0|\mathbf{x}_t]$ by replacing the range space component of $\mathbb{E}[\mathbf{x}_0|\mathbf{x}_t]$ with $\mathbf{A}^\dagger\mathbf{y}$ but keeping the null space component unchanged. We find that, when the measurement noise σ vanishes, replacing the range space component $\mathbf{A}^\dagger\mathbf{A}\mathbb{E}[\mathbf{x}_0|\mathbf{x}_t]$ with $\mathbf{A}^\dagger\mathbf{y}$ is equivalent to replacing $\mathbb{E}[\mathbf{x}_0|\mathbf{x}_t]$ with $\mathbb{E}_q[\mathbf{x}_0|\mathbf{x}_t, \mathbf{y}]$. Therefore, DDNM is equivalent to approximating $p_t(\mathbf{x}_0|\mathbf{x}_t)$ using an isotropic Gaussian, as formalized in Proposition 2.

³ $p_t(\mathbf{y}|\mathbf{x}_0, \mathbf{x}_t) = p(\mathbf{y}|\mathbf{x}_0)$ since we leverage the conditional independence between \mathbf{y} and \mathbf{x}_t given \mathbf{x}_0 .

Proposition 2. For any $r_t > 0$, $\mathbb{E}_q[\mathbf{x}_0|\mathbf{x}_t, \mathbf{y}]$ approaches $\hat{\mathbf{x}}_0^{(t)}$ used in DDNM as the variance of measurement noise approaches zero. Formally, we have

$$\lim_{\sigma \rightarrow 0} \mathbb{E}_q[\mathbf{x}_0|\mathbf{x}_t, \mathbf{y}] = \mathbf{A}^\dagger\mathbf{y} + (\mathbf{I} - \mathbf{A}^\dagger\mathbf{A})\mathbb{E}[\mathbf{x}_0|\mathbf{x}_t]. \quad (11)$$

Proof. Please refer to Appendix A.3. \square

3.3. Solving Inverse Problems With Optimal Posterior Covariance

In Sections 3.1 and 3.2, we unify existing zero-shot diffusion-based solvers with the interpretation of isotropic Gaussian approximations to the intractable posterior distributions $p_t(\mathbf{x}_0|\mathbf{x}_t)$. This unified interpretation motivates us to further optimize the posterior covariance in the Gaussian approximation for enhancing existing diffusion-based solvers. Specifically, we consider to approximate $p_t(\mathbf{x}_0|\mathbf{x}_t)$ using variational Gaussian $q_t(\mathbf{x}_0|\mathbf{x}_t) = \mathcal{N}(\mathbf{x}_0|\boldsymbol{\mu}_t(\mathbf{x}_t), \boldsymbol{\Sigma}_t(\mathbf{x}_t))$ with learnable covariance $\boldsymbol{\Sigma}_t(\mathbf{x}_t)$. In the pre-training stage, $q_t(\mathbf{x}_0|\mathbf{x}_t)$ is learned by minimizing the weighted integral of expected forward KL divergence between $p_t(\mathbf{x}_0|\mathbf{x}_t)$ and $q_t(\mathbf{x}_0|\mathbf{x}_t)$ as

$$\min_q \int \omega_t \mathbb{E}_{p_t(\mathbf{x}_t)} [D_{KL}(p_t(\mathbf{x}_0|\mathbf{x}_t) \| q_t(\mathbf{x}_0|\mathbf{x}_t))] dt. \quad (12)$$

Equation 12 can be achieved in a tractable way by maximizing the log-likelihood of $q_t(\mathbf{x}_0|\mathbf{x}_t)$. When $\boldsymbol{\Sigma}_t(\mathbf{x}_t)$ is full rank, the optimal $\boldsymbol{\mu}_t(\mathbf{x}_t)$ is exactly the MMSE estimator $\mathbb{E}[\mathbf{x}_0|\mathbf{x}_t]$. Once $q_t(\mathbf{x}_0|\mathbf{x}_t)$ is learned, we can leverage $\boldsymbol{\mu}_t$ and $\boldsymbol{\Sigma}_t$ to solve inverse problems and accommodate to existing methods by plugging $\boldsymbol{\mu}_t(\mathbf{x}_t)$ in equation 2 to achieve unconditional sampling. The solutions to Type I and Type II guidance are summarized as below.

Type I guidance. The likelihood is approximated in a similar way to equation 8 using $\boldsymbol{\mu}_t$ and $\boldsymbol{\Sigma}_t$:

$$p_t(\mathbf{y}|\mathbf{x}_t) \approx \mathcal{N}(\mathbf{y}|\mathbf{A}\boldsymbol{\mu}_t(\mathbf{x}_t), \sigma^2\mathbf{I} + \mathbf{A}\boldsymbol{\Sigma}_t(\mathbf{x}_t)\mathbf{A}^T). \quad (13)$$

Type II guidance. $\hat{\mathbf{x}}_0^{(t)}$ is solved from the *auto-weighted* proximal problem associated with $\boldsymbol{\mu}_t$ and $\boldsymbol{\Sigma}_t$:

$$\hat{\mathbf{x}}_0^{(t)} = \arg \min_{\mathbf{x}_0} \|\mathbf{y} - \mathbf{A}\mathbf{x}_0\|^2 + \sigma^2 \|\mathbf{x}_0 - \boldsymbol{\mu}_t(\mathbf{x}_t)\|_{\boldsymbol{\Sigma}_t^{-1}(\mathbf{x}_t)}^2, \quad (14)$$

where $\|\mathbf{x}\|_{\boldsymbol{\Lambda}}^2 = \mathbf{x}^T\boldsymbol{\Lambda}\mathbf{x}$ with positive definite matrix $\boldsymbol{\Lambda}$.

To avoid the inversion of high-dimensional matrices for realizing guidances in practice, we develop closed-form solutions for Type I guidance in equation 13 and Type II guidance in equation 14 under the isotropic posterior covariance $\boldsymbol{\Sigma}_t(\mathbf{x}_t) = r_t^2(\mathbf{x}_t)\mathbf{I}$, as well as numerical solutions based on conjugate gradient method (CG) for more general covariance. Please refer to Appendices B and C for details.

4. Plug-and-Play Posterior Covariance Optimization

Since training diffusion models from scratch using equation 12 is expensive, directly leveraging available checkpoints of unconditional diffusion models is prevailing in prior works. To achieve plug-and-play posterior covariance optimization without retraining, it is non-trivial to obtain posterior covariance prediction from unconditional diffusion models, which has yet to be explored in existing methods. In this section, we develop two alternative ways to achieve optimal *diagonal* posterior covariance without retraining for two common cases: 1) reverse covariance prediction is available from the given unconditional diffusion model (Section 4.1), and 2) reverse covariance prediction is not available (Section 4.2). We also discuss the relation between this paper and the concurrent work (Boys et al., 2023). It is worth noting that, this paper focuses on optimizing diagonal posterior covariance to accommodate existing unconditional diffusion models. Nevertheless, we demonstrate in Appendix D.5 that the proposed method has the potential for generalizing to correlated (non-diagonal) posterior covariance. We will further explore this problem in the future.

4.1. Converting Optimal Reverse Variances

Recent pre-trained diffusion models often predict the optimal *reverse variances*⁴ (Nichol & Dhariwal, 2021) for improving performance when using ancestral sampling of *discrete* diffusion models (or denoising diffusion probabilistic models (DDPM) (Ho et al., 2020; Sohl-Dickstein et al., 2015)). Here, we develop a solution that can directly leverage off-the-shelf reverse covariance prediction based on the fixed-point solution of DDPM to obtain posterior covariance prediction solved from equation 12 and avoid retraining. We first develop the fixed-point solutions to equation 12 under diagonal posterior covariance case in Proposition 3, and then establish the relation between the fixed-point solutions to equation 12 and DDPM in equation 19 in Theorem 4.

Proposition 3 (Fixed-point solutions of variational Gaussian posterior). *The optimal mean $\boldsymbol{\mu}_t^*(\mathbf{x}_t)$ and the optimal diagonal posterior covariances $\boldsymbol{\Sigma}_t^*(\mathbf{x}_t) = \text{diag}[\mathbf{r}_t^{*2}(\mathbf{x}_t)]$ to equation 12 are obtained by*

$$\boldsymbol{\mu}_t^*(\mathbf{x}_t) = \mathbb{E}[\mathbf{x}_0|\mathbf{x}_t], \quad (15)$$

$$\mathbf{r}_t^{*2}(\mathbf{x}_t) = \mathbb{E}_{p_t(\mathbf{x}_0|\mathbf{x}_t)}[(\mathbf{x}_0 - \mathbb{E}[\mathbf{x}_0|\mathbf{x}_t])^2]. \quad (16)$$

Proof. Please refer to Appendix A.5. \square

Subsequently, we consider the fixed-point solutions of DDPM. Unlike continuous ODE formulation introduced in Section 2.2, diffusion models pre-trained under the DDPM

framework are latent variable models defined by $p(\mathbf{x}_0) = \int p(\mathbf{x}_{0:T})d\mathbf{x}_{1:T}$. The joint distribution $p(\mathbf{x}_{0:T})$ is referred to as the *reverse process* defined as a Markov chain of learnable Gaussian transitions starting at $p(\mathbf{x}_T) = \mathcal{N}(\mathbf{0}, \mathbf{I})$ (Ho et al., 2020). The Gaussian transition at time t is characterized by the mean \mathbf{m}_t and covariance \mathbf{C}_t dependent on the condition \mathbf{x}_t :

$$p(\mathbf{x}_{0:T}) = p(\mathbf{x}_T) \prod_{t=1}^T p(\mathbf{x}_{t-1}|\mathbf{x}_t), \quad (17)$$

$$p(\mathbf{x}_{t-1}|\mathbf{x}_t) = \mathcal{N}(\mathbf{x}_{t-1}|\mathbf{m}_t(\mathbf{x}_t), \mathbf{C}_t(\mathbf{x}_t)). \quad (18)$$

DDPM defines a forward process $q(\mathbf{x}_{1:T}|\mathbf{x}_0)$ by gradually injecting noise to the data. Please refer to Appendix A.4 for the detailed definition of $q(\mathbf{x}_{1:T}|\mathbf{x}_0)$. We fit $p(\mathbf{x}_0)$ to the original data distribution $q(\mathbf{x}_0)$ by minimizing the KL divergence between the forward and reverse processes:

$$\min_p D_{KL}(q(\mathbf{x}_{0:T})||p(\mathbf{x}_{0:T})), \quad (19)$$

where $q(\mathbf{x}_{0:T}) = q(\mathbf{x}_0)q(\mathbf{x}_{1:T}|\mathbf{x}_0)$.

In Theorem 4, we present the fixed-point solution of DDPM under signal-dependent diagonal covariance $\mathbf{C}_t(\mathbf{x}_t) = \text{diag}[\mathbf{v}_t^2(\mathbf{x}_t)]$ as used in (Nichol & Dhariwal, 2021).

Theorem 4 (Fixed-point solutions of DDPM). *Let $\mathbf{C}_t(\mathbf{x}_t) = \text{diag}[\mathbf{v}_t^2(\mathbf{x}_t)]$ be a signal-dependent diagonal covariance for the reverse covariance. When $\tilde{\boldsymbol{\mu}}_t, \tilde{\beta}_t, \tilde{\alpha}_t, \tilde{\beta}_t$ are determined by the forward process $q(\mathbf{x}_{1:T}|\mathbf{x}_0)$, the optimal solutions $\mathbf{m}_t^*(\mathbf{x}_t)$ and $\mathbf{v}_t^{*2}(\mathbf{x}_t)$ to equation 19 are*

$$\mathbf{m}_t^*(\mathbf{x}_t) = \tilde{\boldsymbol{\mu}}_t(\mathbf{x}_t, \mathbb{E}[\mathbf{x}_0|\mathbf{x}_t]), \quad (20)$$

$$\mathbf{v}_t^{*2}(\mathbf{x}_t) = \tilde{\beta}_t + \left(\frac{\sqrt{\tilde{\alpha}_{t-1}}\tilde{\beta}_t}{1 - \tilde{\alpha}_t}\right)^2 \cdot \mathbf{r}_t^{*2}(\mathbf{x}_t) \quad (21)$$

where $\mathbf{r}_t^{*2}(\mathbf{x}_t)$ is the optimal posterior variances determined by equation 16 under $s_t = \sqrt{\tilde{\alpha}_t}$ and $\sigma_t = \sqrt{\tilde{\beta}_t/\tilde{\alpha}_t}$, and $\tilde{\beta}_t = (\tilde{\beta}_{t-1}/\tilde{\beta}_t)\beta_t$.

Proof. Please refer to Appendix A.4. \square

Theorem 4 implies that, given the reverse variances $\hat{\mathbf{v}}_t^2(\mathbf{x}_t)$ predicted by a pre-trained DDPM model at time t , the posterior variances are obtained according to equation 21 by

$$\hat{\mathbf{r}}_t^2(\mathbf{x}_t) = (\hat{\mathbf{v}}_t^2(\mathbf{x}_t) - \tilde{\beta}_t) \cdot \left(\frac{\sqrt{\tilde{\alpha}_{t-1}}\tilde{\beta}_t}{1 - \tilde{\alpha}_t}\right)^{-2}. \quad (22)$$

In fact, similar fixed-point solutions of DDPM have been proposed in (Bao et al., 2022b) and (Bao et al., 2022a) for determining optimal reverse variances. Our approach can be viewed as opposite direction to (Bao et al., 2022b) and (Bao et al., 2022a) for applying the fixed-point solutions.

⁴Variances are the diagonal elements of the covariance matrix.

4.2. Monte Carlo Estimation of Posterior Variances

We further develop the optimal posterior variances using a pre-trained unconditional diffusion model without providing the reverse variances prediction $\hat{v}_t^2(\mathbf{x}_t)$ (e.g., (Ho et al., 2020)). In this case, we suppose signal-independent $\Sigma_t(\mathbf{x}_t) = r_t^2 \mathbf{I}$ is an isotropic covariance with a time-dependent standard deviation r_t . We directly optimize r_t by forcing the derivative of equation 12 with an optimal μ_t with regard to r_t to zero. Thus, we obtain that

$$r_t^{*2} = \frac{1}{d} \mathbb{E}_{p_t(\mathbf{x}_0, \mathbf{x}_t)} [\|\mathbf{x}_0 - \mathbb{E}[\mathbf{x}_0 | \mathbf{x}_t]\|^2]. \quad (23)$$

Note that we only estimate the expected reconstruction error of the MMSE estimator $\mathbb{E}[\mathbf{x}_0 | \mathbf{x}_t]$. Similar to (Bao et al., 2022b), given a pre-trained unconditional diffusion model D_t , r_t^{*2} is estimated using Monte Carlo samples as

$$\hat{r}_t^2 = \frac{1}{dM} \sum_{m=1}^M \|\mathbf{x}_0^{(m)} - D_t(\mathbf{x}_t^{(m)})\|_2^2, \quad (24)$$

where $\mathbf{x}_0^{(m)}, \mathbf{x}_t^{(m)} \sim p(\mathbf{x}_0)p_t(\mathbf{x}_t | \mathbf{x}_0)$ and M is the number of Monte Carlo samples. In the discrete-time case, \hat{r}_t^2 is pre-computed for any t and reused in subsequent computations. In the continuous-time case, we pre-compute \hat{r}_t^2 for 1000 discrete time steps, and for any t used in sampling, we use the pre-computed result with the nearest time step to t .

4.3. Comparison With Tweedie Moment Projection

Concurrent to our work, Boys et al. (2023) also leverage the idea of optimizing posterior covariance for solving inverse problems. Specifically, they leverage second-order Tweedie’s formula to achieve posterior covariance optimization: $\Sigma^*(\mathbf{x}_t) = \sigma_t^2 \nabla_{\mathbf{x}_t} \mathbb{E}[\mathbf{x}_0 | \mathbf{x}_t]$, where $\Sigma_t^*(\mathbf{x}_t)$ is the optimal $\Sigma_t(\mathbf{x}_t)$ for equation 12 and $\nabla_{\mathbf{x}_t} \mathbb{E}[\mathbf{x}_0 | \mathbf{x}_t]$ is the Jacobian of $\mathbb{E}[\mathbf{x}_0 | \mathbf{x}_t]$. However, without strong approximation, their approach cannot scale to high dimensional data like images. In particular, they leverage row sum approximation for the Jacobian: $\nabla_{\mathbf{x}_t} \mathbb{E}[\mathbf{x}_0 | \mathbf{x}_t] \approx \text{diag}[\nabla_{\mathbf{x}_t} \mathbf{1}^T \mathbb{E}[\mathbf{x}_0 | \mathbf{x}_t]]$ for image experiments. In contrast, we achieve posterior covariance optimization without introducing additional computational cost, as elaborated in Sections 4.1 and 4.2.

5. Experiments

We implement our techniques and re-implement prior works on a newly written codebase based on an open-source diffusion codebase k-diffusion⁵. This allows us to minimize the effect of different implementations for fair comparison and allows prior works to use a more advanced sampler that is not supported by the original codebase. Following (Chung et al., 2023; Wang et al., 2023), we perform experiments

⁵<https://github.com/crowsonkb/k-diffusion>

Task	Avg. MAD
Inpaint (Random)	1.6975×10^{-6}
Deblur (Gaussian)	6.4629×10^{-4}
Deblur (Motion)	1.5461×10^{-3}
Super resolution (4×)	1.1937×10^{-2}

Table 2: **DDNM v.s. DiffPIR in noiseless inverse problems.** We report the averaged MAD between their $\mathbf{x}_0^{(t)}$ averaged over all sampling steps and test images.

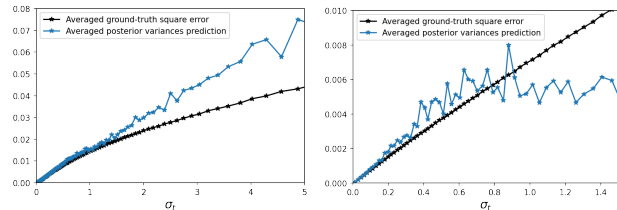


Figure 1: **Averaged values of e (black line) and $r_t^2(\mathbf{x}_t)$ (blue line) on FFHQ (Left) and ImageNet (Right).**

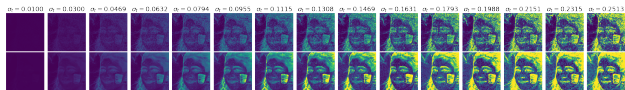


Figure 2: **Visualization of e and $\hat{r}_t^2(\mathbf{x}_t)$ of an example image \mathbf{x}_0 at different t .** Top: e ; Bottom: $\hat{r}_t^2(\mathbf{x}_t)$. The results are averaged over RGB channels for better visualization.

on the FFHQ 256×256 and ImageNet 256×256 datasets to compare different methods. For each dataset, we report the average results over 100 validation images. Following (Chung et al., 2023; Zhu et al., 2023), we use the pre-trained unconditional diffusion models from (Dhariwal & Nichol, 2021) and (Chung et al., 2023) for ImageNet and FFHQ datasets, respectively.

The degradation models are specified mostly following (Zhu et al., 2023): (i) For inpainting, we randomly mask 50 percent of the total pixels. (ii) For Gaussian deblurring and motion deblurring, we use the same setup of the blurring kernels to (Chung et al., 2023). (iii) For super resolution (SR), we consider bicubic downsampling. All measurements are corrupted by Gaussian noise with $\sigma = 0.05$. See Appendix D for more experimental details and results.

5.1. Validation of Theoretical Results

DDNM as noiseless DiffPIR. To validate Proposition 2, we re-implement DDNM under DiffPIR codebase. DiffPIR deals with noiseless inverse problems by setting σ to a relatively low value for ρ_t in equation 9 (e.g., 0.001 in DiffPIR codebase). We demonstrate that directly using the DDNM solution in equation 11 produces similar results in

Dataset	Method	Inpaint (Random)			Deblur (Gaussian)			Deblur (Motion)			Super resolution (4×)		
		SSIM ↑	LPIPS ↓	FID ↓	SSIM ↑	LPIPS ↓	FID ↓	SSIM ↑	LPIPS ↓	FID ↓	SSIM ↑	LPIPS ↓	FID ↓
FFHQ	Convert (<i>Ours</i>)	0.9279	0.0794	25.90	0.7905	0.1836	52.42	0.7584	0.2156	62.88	0.7878	0.1962	58.37
	Analytic (<i>Ours</i>)	<u>0.9272</u>	<u>0.0845</u>	<u>28.83</u>	0.7926	<u>0.1850</u>	<u>53.09</u>	<u>0.7579</u>	<u>0.2183</u>	<u>64.77</u>	0.7878	<u>0.1968</u>	<u>59.83</u>
	TMPD	0.8224	0.1924	70.92	0.7289	0.2523	76.52	0.7014	0.2718	83.49	0.7085	0.2701	79.58
	DPS	0.8891	0.1323	49.46	0.6284	0.3652	136.12	0.4904	0.4924	212.48	0.7719	0.2054	61.36
	IGDM	0.8784	0.1422	49.89	0.7890	0.1910	59.93	0.7543	0.2209	66.14	0.7850	0.2005	61.46
ImageNet	Convert (<i>Ours</i>)	<u>0.8559</u>	0.1329	29.14	0.6007	0.3327	<u>95.23</u>	0.5634	0.3656	109.61	0.5869	<u>0.3477</u>	96.76
	Analytic (<i>Ours</i>)	<u>0.8481</u>	<u>0.1446</u>	<u>35.51</u>	0.6009	<u>0.3334</u>	93.21	<u>0.5611</u>	<u>0.3668</u>	<u>113.39</u>	0.5958	<u>0.3495</u>	<u>95.33</u>
	TMPD	0.7011	0.2892	293.80	0.5430	0.4114	291.29	0.4773	0.4567	302.40	0.5186	0.4298	296.73
	DPS	0.8623	0.1490	36.58	0.4603	0.4630	173.77	0.3582	0.5554	282.21	0.5860	0.3231	92.89
	IGDM	0.7658	0.2328	64.96	0.5946	0.3429	102.89	0.5534	0.3781	113.89	<u>0.5925</u>	<u>0.3552</u>	100.36

Table 3: **Quantitative results on FFHQ and ImageNet dataset for Type I guidance.** We use **bold** and underline for the best and second best, respectively.

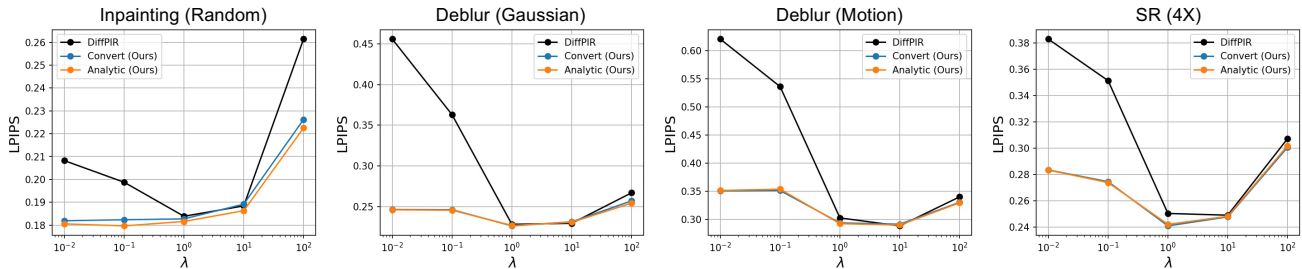


Figure 3: **LPIPS comparisons on FFHQ for Type II guidance.** We report LPIPS under different λ .

the noiseless case. Table 2 reports the Mean Absolute Difference (MAD)⁶ between the conditional posterior means in equations 9 and 11 by averaging over all the sampling steps and test images. Overall, the MAD is negligible in comparison to the data range of $[-1, 1]$. Deblurring and super resolution yield larger MAD than inpainting, since several approximations are made for computing A^\dagger , while for inpainting A^\dagger is exact (see Appendix D.3 for details).

Sanity check to equation 22. To validate the effectiveness of equation 22 in practice, we compare the ground-truth square errors made by the denoiser $e = (x_0 - D_t(x_t))^2$ with the posterior variance prediction $\hat{r}_t^2(x_t)$. We compare e with $\hat{r}_t^2(x_t)$ since the posterior variance $r_t^{*2}(x_t)$ is the MMSE estimator of e given x_t (assuming $D_t(x_t) = \mathbb{E}[x_0|x_t]$), as suggested by equation 16. This implies that a good $\hat{r}_t^2(x_t)$ should be a reliable predictor of e . Thus, we compare e with $\hat{r}_t^2(x_t)$ as a sanity check to gauge the effectiveness of equation 22 in practice. In Figure 1, we plot their averaged values over all the pixels and test images. The posterior variances prediction obtained via equation 22 is accurate only in the regions with low noise level. This is reasonable since the optimal reverse variance $v^{*2}(x_t)$ is bounded by the upper bound β_t and the lower bound $\tilde{\beta}_t$. The two bounds are almost equal in the regions with high noise level (Nichol & Dhariwal, 2021). When t is large,

⁶MAD between x and y is defined by $\|x - y\|_1/d$.

$v^{*2}(x_t) - \tilde{\beta}_t \approx 0$ and equation 22 becomes a 0/0 limit that possesses high numerical instability. In Figure 2, we visualize e and $\hat{r}_t^2(x_t)$ of an image x_0 at different t and show that e can be well predicted by $\hat{r}_t^2(x_t)$ when t is small.

5.2. Quantitative Results

Experimental setup. To evaluate different methods, we follow Chung et al. (2023) to use three metrics: Structure Similarity Index Measure (SSIM), Learned Perceptual Image Patch Similarity (LPIPS, Zhang et al. (2018)) and Fréchet Inception Distance (FID, Heusel et al. (2017)). All Type I guidance methods use the same Heun’s 2nd deterministic sampler suggested in Karras et al. (2022) with 50 sampling steps, and all Type II guidance methods use the same Heun’s 2nd stochastic sampler ($S_{\text{churn}} = 80, S_{\text{tmin}} = 0.05, S_{\text{tmax}} = 1, S_{\text{noise}} = 1.007$, definition see Karras et al. (2022)) with 50 sampling steps since we found that Type II guidance does not perform well using deterministic samplers⁷.

In initial experiments, using our optimal posterior covariance for all sampling steps results in poor performance. This may due to Gaussian variational $q_t(x_0|x_t)$ is an effective approximation to posterior $p_t(x_0|x_t)$ only for small noise level (Xiao et al., 2022). To address this, we heuristically

⁷To understand how to leverage pre-trained DDPM model to perform sampling under perturbation kernels given in Section 2.2, please refer to Appendix D.2.

Dataset	Method	Inpaint (Random)			Deblur (Gaussian)			Deblur (Motion)			Super resolution (4×)		
		SSIM ↑	LPIPS ↓	FID ↓	SSIM ↑	LPIPS ↓	FID ↓	SSIM ↑	LPIPS ↓	FID ↓	SSIM ↑	LPIPS ↓	FID ↓
FFHQ	Convert (<i>Ours</i>)	0.9241	0.0822	27.50	0.7783	0.1969	59.31	0.7329	0.2324	66.18	0.7632	0.2183	67.17
	Analytic (<i>Ours</i>)	<u>0.9232</u>	<u>0.0852</u>	<u>28.63</u>	0.7790	0.1971	<u>59.80</u>	0.7331	<u>0.2336</u>	<u>69.82</u>	<u>0.7622</u>	<u>0.2195</u>	<u>68.84</u>
	ΠIGDM	0.7078	0.2605	77.46	0.7221	0.2421	71.19	0.6977	0.2607	75.15	0.7205	0.2442	72.41
ImageNet	Convert (<i>Ours</i>)	0.8492	0.1394	33.46	0.5770	0.3568	100.50	0.5341	0.3944	131.48	0.5613	0.3846	116.27
	Analytic (<i>Ours</i>)	<u>0.8417</u>	<u>0.1484</u>	<u>37.98</u>	<u>0.5722</u>	<u>0.3583</u>	<u>103.67</u>	0.5341	<u>0.3947</u>	126.39	<u>0.5537</u>	<u>0.3867</u>	<u>116.87</u>
	ΠIGDM	0.5102	0.4293	141.80	0.5071	0.4095	127.41	0.4887	0.4267	132.38	0.5150	0.4098	127.40

Table 4: Results for ΠIGDM with adaptive weight on FFHQ and ImageNet dataset. We use bold and underline for the best and second best, respectively.

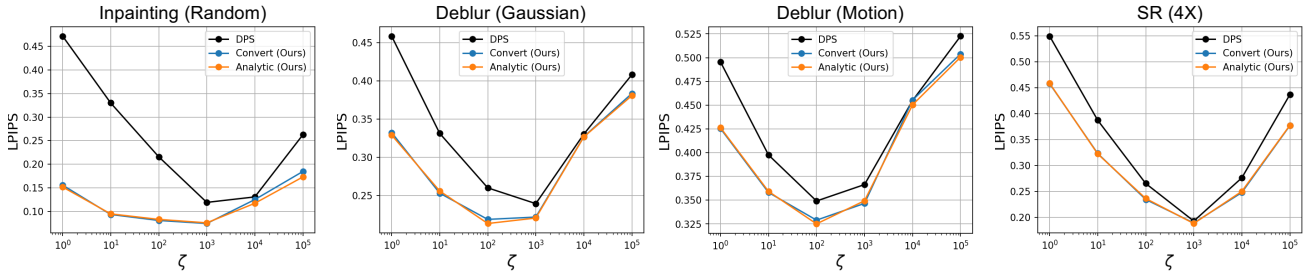


Figure 4: LPIPS comparisons on FFHQ for DPS with heuristic guidance strength. We report LPIPS under different ζ .

use the optimal posterior covariance only at the last several sampling steps with low noise level but use ΠIGDM and DiffPIR covariances for Type I and Type II guidance for high noise level, respectively. We empirically find that sampling with our optimal covariance yields highly stable results when $\sigma_t < 0.2$ (*i.e.*, 12 out of 50 steps).

Results for pure covariance comparisons. Table 3 summarizes the results for Type I guidance. DPS and ΠIGDM refer to the posterior covariance type discussed in Section 3.1; Convert, Analytic, and TMPD refer to the posterior covariance type obtained using approaches presented in Sections 4.1, 4.2, and 4.3, respectively. Note that for Type I guidance, our methods achieve the best results in almost all tasks. Although DPS outperforms us in several cases, we observe that its performance is very unstable (see DPS performance in deblurring tasks). For Type II guidance, since we use DiffPIR covariance in high noise level region, the performance of our method and DiffPIR baseline are both influenced by the hyper-parameter λ . Therefore, we report the performance under different λ in Figure 3. Our method is more robust than DiffPIR to the hyper-parameter λ , which demonstrates that the last sampling steps are near optimal when using optimal posterior covariance.

Results with heuristics implementations. Prior works propose several heuristics to enhance performance, in addition to using Gaussian for posterior approximation. The results in Table 3 are based on re-implementations that exclude these heuristics for pure covariance comparisons. We further investigate the effectiveness of our techniques by applying

them to the last sampling steps of these re-implementations.

ΠIGDM introduces an *adaptive weight* to the likelihood score $\nabla_{\mathbf{x}_t} \log p_t(\mathbf{y}|\mathbf{x}_t)$ to adjust the guidance strength according to the timestep. Specifically, the likelihood score is substituted with $r_t^2 \nabla_{\mathbf{x}_t} \log p_t(\mathbf{y}|\mathbf{x}_t)$ with $r_t^2 = \sigma_t^2 / (1 + \sigma_t^2)$. Table 4 summarizes the results for ΠIGDM with adaptive weight. Obviously, ΠIGDM achieves significant performance gain using Type I guidance with optimal variances at the last sampling steps. As for DPS, it introduces a trick to heuristically determine the strength of guidance as mentioned in Section 3.1. Since this trick involves a hyper-parameter ζ , we report the performance under different ζ . Figure 4 summarizes the quantitative results for DPS with heuristic guidance strength. DPS with the last sampling steps replaced by our techniques can achieve the best results across all hyper-parameters.

6. Conclusions

We show that recent diffusion-based inverse problem solvers can be interpreted as isotropic Gaussian approximations to the intractable posterior distributions. Inspired by this, we propose to enhance these existing methods by optimizing the posterior covariances using two novel plug-and-play strategies. Experimental results demonstrate that the proposed methods significantly outperform existing zero-shot methods and enhance the robustness to hyperparameters.

Limitations Despite the reasonable improvements our approaches offer over prior works, it is worth noting that the Gaussian assumption with a diagonal covariance might be an oversimplification to approximate the true pixel-correlated image posterior. This could potentially limit the performance. Future research could explore better principles for designing the covariance, such as leveraging orthogonal transformation for correlation reduction (see Appendix D.5 for discussion). Additionally, methods like efficient approximation for Tweedie moment projection could be investigated. These represent intriguing directions for future work.

References

- Ballé, J., Chou, P. A., Minnen, D., Singh, S., Johnston, N., Agustsson, E., Hwang, S. J., and Toderici, G. Nonlinear transform coding. *IEEE Journal of Selected Topics in Signal Processing*, 15(2):339–353, 2020.
- Bao, F., Li, C., Sun, J., Zhu, J., and Zhang, B. Estimating the optimal covariance with imperfect mean in diffusion probabilistic models. In *Proceedings of the 39th International Conference on Machine Learning*, pp. 1555–1584, 2022a.
- Bao, F., Li, C., Zhu, J., and Zhang, B. Analytic-DPM: an analytic estimate of the optimal reverse variance in diffusion probabilistic models. In *The 10th International Conference on Learning Representations*, 2022b. URL <https://openreview.net/forum?id=0xiJLKH-ufz>.
- Bishop, C. M. *Pattern Recognition and Machine Learning*. Springer, 2006.
- Boys, B., Girolami, M., Pidstrigach, J., Reich, S., Mosca, A., and Akyildiz, O. D. Tweedie moment projected diffusions for inverse problems. *arXiv preprint arXiv:2310.06721*, 2023.
- Chan, M. A., Young, S. I., and Metzler, C. A. SUD²: Supervision by denoising diffusion models for image reconstruction. In *NeurIPS 2023 Deep Inverse Workshop*, 2023.
- Choi, J., Kim, S., Jeong, Y., Gwon, Y., and Yoon, S. Ilvr: Conditioning method for denoising diffusion probabilistic models. *arXiv preprint arXiv:2108.02938*, 2021.
- Chung, H., Kim, J., Mccann, M. T., Klasky, M. L., and Ye, J. C. Diffusion posterior sampling for general noisy inverse problems. In *The 11th International Conference on Learning Representations*, 2023. URL <https://openreview.net/forum?id=OnD9zGAGT0k>.
- Dhariwal, P. and Nichol, A. Diffusion models beat GANs on image synthesis. In *Advances in Neural Information Processing Systems 34*, pp. 8780–8794, 2021.
- Feng, B. T., Smith, J., Rubinstein, M., Chang, H., Bouman, K. L., and Freeman, W. T. Score-based diffusion models as principled priors for inverse imaging. In *Proceedings of the IEEE/CVF International Conference on Computer Vision*, pp. 10520–10531, 2023.
- Hestenes, M. R., Stiefel, E., et al. Methods of conjugate gradients for solving linear systems. *Journal of research of the National Bureau of Standards*, 49(6):409–436, 1952.
- Heusel, M., Ramsauer, H., Unterthiner, T., Nessler, B., and Hochreiter, S. Gans trained by a two time-scale update rule converge to a local nash equilibrium. In *Advances in Neural Information Processing Systems 30*, 2017.
- Ho, J., Jain, A., and Abbeel, P. Denoising diffusion probabilistic models. In *Advances in Neural Information Processing Systems 33*, pp. 6840–6851, 2020.
- Karras, T., Aittala, M., Aila, T., and Laine, S. Elucidating the design space of diffusion-based generative models. In *Advances in Neural Information Processing Systems 35*, pp. 26565–26577, 2022.
- Kingma, D., Salimans, T., Poole, B., and Ho, J. Variational diffusion models. In *Advances in Neural Information Processing Systems 34*, pp. 21696–21707, 2021.
- Lugmayr, A., Danelljan, M., Romero, A., Yu, F., Timofte, R., and Van Gool, L. Repaint: Inpainting using denoising diffusion probabilistic models. In *Proceedings of the IEEE/CVF Conference on Computer Vision and Pattern Recognition*, pp. 11461–11471, 2022.
- Luo, Z., Gustafsson, F. K., Zhao, Z., Sjölund, J., and Schön, T. B. Refusion: Enabling large-size realistic image restoration with latent-space diffusion models. In *Proceedings of the IEEE/CVF Conference on Computer Vision and Pattern Recognition*, pp. 1680–1691, 2023.
- Mardani, M., Song, J., Kautz, J., and Vahdat, A. A variational perspective on solving inverse problems with diffusion models. *arXiv preprint arXiv:2305.04391*, 2023.
- Nichol, A. Q. and Dhariwal, P. Improved denoising diffusion probabilistic models. In *Proceedings of the 38th International Conference on Machine Learning*, pp. 8162–8171, 2021.
- Pokle, A., Muckley, M. J., Chen, R. T., and Karrer, B. Training-free linear image inversion via flows. *arXiv preprint arXiv:2310.04432*, 2023.
- Ravula, S., Levac, B., Jalal, A., Tamir, J. I., and Dimakis, A. G. Optimizing sampling patterns for compressed sensing MRI with diffusion generative models. *arXiv preprint arXiv:2306.03284*, 2023.

-
- Rezende, D. J. and Viola, F. Taming VAEs. *arXiv preprint arXiv:1810.00597*, 2018.
- Saharia, C., Ho, J., Chan, W., Salimans, T., Fleet, D. J., and Norouzi, M. Image super-resolution via iterative refinement. *IEEE Transactions on Pattern Analysis and Machine Intelligence*, 45(4):4713–4726, 2022.
- Sohl-Dickstein, J., Weiss, E., Maheswaranathan, N., and Ganguli, S. Deep unsupervised learning using nonequilibrium thermodynamics. In *Proceeding of the 35th International Conference on Machine Learning*, pp. 2256–2265, 2015.
- Song, J., Meng, C., and Ermon, S. Denoising diffusion implicit models. In *The 9th International Conference on Learning Representations*, 2021a. URL <https://openreview.net/forum?id=St1giarCHLP>.
- Song, J., Vahdat, A., Mardani, M., and Kautz, J. Pseudoinverse-guided diffusion models for inverse problems. In *The 11th International Conference on Learning Representations*, 2023. URL https://openreview.net/forum?id=9_gsMA8MRKQ.
- Song, Y. and Ermon, S. Generative modeling by estimating gradients of the data distribution. In *Advances in Neural Information Processing Systems 32*, 2019.
- Song, Y., Sohl-Dickstein, J., Kingma, D. P., Kumar, A., Ermon, S., and Poole, B. Score-based generative modeling through stochastic differential equations. In *The 9th International Conference on Learning Representations*, 2021b. URL <https://openreview.net/forum?id=PxtTIG12RRHS>.
- Song, Y., Shen, L., Xing, L., and Ermon, S. Solving inverse problems in medical imaging with score-based generative models. In *The 10th International Conference on Learning Representations*, 2022. URL <https://openreview.net/forum?id=vaRCHVj0uGI>.
- Wang, Y., Yu, J., and Zhang, J. Zero-shot image restoration using denoising diffusion null-space model. In *The 11th International Conference on Learning Representations*, 2023. URL <https://openreview.net/forum?id=mRieQgMtNTQ>.
- Whang, J., Delbracio, M., Talebi, H., Saharia, C., Dimakis, A. G., and Milanfar, P. Deblurring via stochastic refinement. In *Proceedings of the IEEE/CVF Conference on Computer Vision and Pattern Recognition*, pp. 16293–16303, 2022.
- Xiao, Z., Kreis, K., and Vahdat, A. Tackling the generative learning trilemma with denoising diffusion GANs. In *The 10th International Conference on Learning Representations*, 2022. URL <https://openreview.net/forum?id=JprM0p-q0Co>.
- Zhang, K., Gool, L. V., and Timofte, R. Deep unfolding network for image super-resolution. In *Proceedings of the IEEE/CVF Conference on Computer Vision and Pattern Recognition*, pp. 3217–3226, 2020.
- Zhang, R., Isola, P., Efros, A. A., Shechtman, E., and Wang, O. The unreasonable effectiveness of deep features as a perceptual metric. In *Proceedings of the IEEE Conference on Computer Vision and Pattern Recognition*, pp. 586–595, 2018.
- Zhu, Y., Zhang, K., Liang, J., Cao, J., Wen, B., Timofte, R., and Van Gool, L. Denoising diffusion models for plug-and-play image restoration. In *Proceedings of the IEEE/CVF Conference on Computer Vision and Pattern Recognition*, pp. 1219–1229, 2023.

A. Proofs to Theoretical Results

Lemma 5 (Tweedie’s formula). *If the joint distribution between $\mathbf{x}_0, \mathbf{x}_t$ is given by $p_t(\mathbf{x}_0, \mathbf{x}_t) = p(\mathbf{x}_0)p_t(\mathbf{x}_t|\mathbf{x}_0)$ with $p_t(\mathbf{x}_t|\mathbf{x}_0) = \mathcal{N}(\mathbf{x}_t|s_t\mathbf{x}_0, s_t^2\sigma_t^2\mathbf{I})$, then $\nabla_{\mathbf{x}_t} \log p_t(\mathbf{x}_t) = \frac{1}{s_t^2\sigma_t^2}(s_t\mathbb{E}[\mathbf{x}_0|\mathbf{x}_t] - \mathbf{x}_t)$.*

Proof.

$$\nabla_{\mathbf{x}_t} \log p_t(\mathbf{x}_t) = \frac{\nabla_{\mathbf{x}_t} p_t(\mathbf{x}_t)}{p_t(\mathbf{x}_t)} \quad (25)$$

$$= \frac{1}{p_t(\mathbf{x}_t)} \nabla_{\mathbf{x}_t} \int p(\mathbf{x}_0)p_t(\mathbf{x}_t|\mathbf{x}_0)d\mathbf{x}_0 \quad (26)$$

$$= \frac{1}{p_t(\mathbf{x}_t)} \int p(\mathbf{x}_0)\nabla_{\mathbf{x}_t} p_t(\mathbf{x}_t|\mathbf{x}_0)d\mathbf{x}_0 \quad (27)$$

$$= \frac{1}{p_t(\mathbf{x}_t)} \int p(\mathbf{x}_0)p_t(\mathbf{x}_t|\mathbf{x}_0)\nabla_{\mathbf{x}_t} \log p_t(\mathbf{x}_t|\mathbf{x}_0)d\mathbf{x}_0 \quad (28)$$

$$= \int p_t(\mathbf{x}_0|\mathbf{x}_t)\nabla_{\mathbf{x}_t} \log p_t(\mathbf{x}_t|\mathbf{x}_0)d\mathbf{x}_0 \quad (29)$$

$$= \mathbb{E}_{p_t(\mathbf{x}_0|\mathbf{x}_t)}[\nabla_{\mathbf{x}_t} \log p_t(\mathbf{x}_t|\mathbf{x}_0)] \quad (30)$$

For Gaussian perturbation kernel $p_t(\mathbf{x}_t|\mathbf{x}_0) = \mathcal{N}(\mathbf{x}_t|s_t\mathbf{x}_0, s_t^2\sigma_t^2\mathbf{I})$, we have $\nabla_{\mathbf{x}_t} \log p_t(\mathbf{x}_t|\mathbf{x}_0) = \frac{1}{s_t^2\sigma_t^2}(s_t\mathbf{x}_0 - \mathbf{x}_t)$. Plug it into equation 30, we conclude the proof. \square

Lemma 6 (Conditional Tweedie’s formula). *If the joint distribution between $\mathbf{x}_0, \mathbf{y}, \mathbf{x}_t$ is given by $p_t(\mathbf{x}_0, \mathbf{y}, \mathbf{x}_t) = p(\mathbf{x}_0)p(\mathbf{y}|\mathbf{x}_0)p_t(\mathbf{x}_t|\mathbf{x}_0)$ with $p_t(\mathbf{x}_t|\mathbf{x}_0) = \mathcal{N}(\mathbf{x}_t|s_t\mathbf{x}_0, s_t^2\sigma_t^2\mathbf{I})$, then $\nabla_{\mathbf{x}_t} \log p_t(\mathbf{x}_t|\mathbf{y}) = \frac{1}{s_t^2\sigma_t^2}(s_t\mathbb{E}[\mathbf{x}_0|\mathbf{x}_t, \mathbf{y}] - \mathbf{x}_t)$.*

Proof.

$$\nabla_{\mathbf{x}_t} \log p_t(\mathbf{x}_t|\mathbf{y}) = \frac{\nabla_{\mathbf{x}_t} p_t(\mathbf{x}_t|\mathbf{y})}{p_t(\mathbf{x}_t|\mathbf{y})} \quad (31)$$

$$= \frac{1}{p_t(\mathbf{x}_t|\mathbf{y})} \nabla_{\mathbf{x}_t} \int p_t(\mathbf{x}_t|\mathbf{x}_0, \mathbf{y})p(\mathbf{x}_0|\mathbf{y})d\mathbf{x}_0 \quad (32)$$

$$= \frac{1}{p_t(\mathbf{x}_t|\mathbf{y})} \nabla_{\mathbf{x}_t} \int p_t(\mathbf{x}_t|\mathbf{x}_0)p(\mathbf{x}_0|\mathbf{y})d\mathbf{x}_0 \quad (33)$$

$$= \frac{1}{p_t(\mathbf{x}_t|\mathbf{y})} \int p(\mathbf{x}_0|\mathbf{y})\nabla_{\mathbf{x}_t} p_t(\mathbf{x}_t|\mathbf{x}_0)d\mathbf{x}_0 \quad (34)$$

$$= \frac{1}{p_t(\mathbf{x}_t|\mathbf{y})} \int p(\mathbf{x}_0|\mathbf{y})p_t(\mathbf{x}_t|\mathbf{x}_0, \mathbf{y})\nabla_{\mathbf{x}_t} \log p_t(\mathbf{x}_t|\mathbf{x}_0)d\mathbf{x}_0 \quad (35)$$

$$= \int p_t(\mathbf{x}_0|\mathbf{x}_t, \mathbf{y})\nabla_{\mathbf{x}_t} \log p_t(\mathbf{x}_t|\mathbf{x}_0)d\mathbf{x}_0 \quad (36)$$

$$= \mathbb{E}_{p_t(\mathbf{x}_0|\mathbf{x}_t, \mathbf{y})}[\nabla_{\mathbf{x}_t} \log p_t(\mathbf{x}_t|\mathbf{x}_0)] \quad (37)$$

where equation 33 and equation 35 are due to the conditional independence between \mathbf{x}_t and \mathbf{y} given \mathbf{x}_0 , such that $p_t(\mathbf{x}_t|\mathbf{x}_0, \mathbf{y}) = p_t(\mathbf{x}_t|\mathbf{x}_0)$. For Gaussian perturbation kernel $p_t(\mathbf{x}_t|\mathbf{x}_0) = \mathcal{N}(\mathbf{x}_t|s_t\mathbf{x}_0, s_t^2\sigma_t^2\mathbf{I})$, we have $\nabla_{\mathbf{x}_t} \log p_t(\mathbf{x}_t|\mathbf{x}_0) = \frac{1}{s_t^2\sigma_t^2}(s_t\mathbf{x}_0 - \mathbf{x}_t)$. Plug it into equation 37, we conclude the proof. \square

A.1. Derivation of the Marginal Preserving Property of Diffusion ODEs

For the sake of completeness, here we prove that the ODEs given in equation 2 and equation 4 respectively maintain the exact same marginals to $p_t(\mathbf{x}_t)$ and $p_t(\mathbf{x}_t|\mathbf{y})$.

Proof. By borrowing the results from (Equation 4, (Karras et al., 2022)) and setting $s_t = 1, \sigma_t = t, \mathbf{x}_t$ determined by the following ODE preserves the marginal $p_t(\mathbf{x}_t)$ for all $t \in [0, T]$:

$$d\mathbf{x}_t = -t\nabla_{\mathbf{x}_t} \log p_t(\mathbf{x}_t)dt, \quad \mathbf{x}_T \sim p_T(\mathbf{x}_T) \quad (38)$$

Using the posterior mean $\mathbb{E}[\mathbf{x}_0|\mathbf{x}_t]$ to represent the score $\nabla_{\mathbf{x}_t} \log p_t(\mathbf{x}_t)$ using Lemma 5, we recover equation 2:

$$d\mathbf{x}_t = \frac{\mathbf{x}_t - \mathbb{E}[\mathbf{x}_0|\mathbf{x}_t]}{t} dt, \quad \mathbf{x}_T \sim p_T(\mathbf{x}_T) \quad (39)$$

Likewise, the following ODE preserves the marginal $p_t(\mathbf{x}_t|\mathbf{y})$ for all $t \in [0, T]$:

$$d\mathbf{x}_t = -t \nabla_{\mathbf{x}_t} \log p_t(\mathbf{x}_t|\mathbf{y}) dt, \quad \mathbf{x}_T \sim p_T(\mathbf{x}_T|\mathbf{y}) \quad (40)$$

By Lemma 6, we recover equation 4:

$$d\mathbf{x}_t = \frac{\mathbf{x}_t - \mathbb{E}[\mathbf{x}_0|\mathbf{x}_t, \mathbf{y}]}{t} dt, \quad \mathbf{x}_T \sim p_T(\mathbf{x}_T|\mathbf{y}) \quad (41)$$

□

A.2. Proof of Proposition 1

To relate $\mathbb{E}[\mathbf{x}_0|\mathbf{x}_t, \mathbf{y}]$ to $\mathbb{E}[\mathbf{x}_0|\mathbf{x}_t]$, we note that

$$\nabla_{\mathbf{x}_t} \log p_t(\mathbf{x}_t|\mathbf{y}) = \nabla_{\mathbf{x}_t} \log p_t(\mathbf{x}_t) + \nabla_{\mathbf{x}_t} \log p_t(\mathbf{y}|\mathbf{x}_t) \quad (42)$$

Using Lemma 5 and Lemma 6, we have

$$\frac{1}{s_t^2 \sigma_t^2} (s_t \mathbb{E}[\mathbf{x}_0|\mathbf{x}_t, \mathbf{y}] - \mathbf{x}_t) = \frac{1}{s_t^2 \sigma_t^2} (s_t \mathbb{E}[\mathbf{x}_0|\mathbf{x}_t] - \mathbf{x}_t) + \nabla_{\mathbf{x}_t} \log p_t(\mathbf{y}|\mathbf{x}_t) \quad (43)$$

and consequently,

$$\mathbb{E}[\mathbf{x}_0|\mathbf{x}_t, \mathbf{y}] = \mathbb{E}[\mathbf{x}_0|\mathbf{x}_t] + s_t \sigma_t^2 \nabla_{\mathbf{x}_t} \log p_t(\mathbf{y}|\mathbf{x}_t) \quad (44)$$

A.3. Proof of Proposition 2

When $\sigma \rightarrow 0$, finding the minimizer of equation 10 is equivalent to solving the following hard-constraint optimization problem:

$$\min_{\hat{\mathbf{x}}_0} \|\hat{\mathbf{x}}_0 - \mathbb{E}[\mathbf{x}_0|\mathbf{x}_t]\|_2^2 \quad \text{s.t.} \quad \mathbf{y} = \mathbf{A}\hat{\mathbf{x}}_0 \quad (45)$$

We define the Lagrangian $\mathcal{L}(\hat{\mathbf{x}}_0, \lambda) = \frac{1}{2} \|\hat{\mathbf{x}}_0 - \mathbb{E}[\mathbf{x}_0|\mathbf{x}_t]\|_2^2 + \lambda^T (\mathbf{y} - \mathbf{A}\hat{\mathbf{x}}_0)$, where λ is the Lagrangian multiplier. By the optimality condition, we have

$$\nabla_{\hat{\mathbf{x}}_0} \mathcal{L} = \hat{\mathbf{x}}_0 - \mathbb{E}[\mathbf{x}_0|\mathbf{x}_t] - \mathbf{A}^T \lambda = \mathbf{0} \quad (46)$$

$$\nabla_{\lambda} \mathcal{L} = \mathbf{y} - \mathbf{A}\hat{\mathbf{x}}_0 = \mathbf{0} \quad (47)$$

Multiplying \mathbf{A} to equation 46 and combining the condition of equation 47 gives:

$$\mathbf{A}(\hat{\mathbf{x}}_0 - \mathbb{E}[\mathbf{x}_0|\mathbf{x}_t] - \mathbf{A}^T \lambda) = \mathbf{0} \quad (48)$$

$$\Rightarrow \mathbf{y} - \mathbf{A}\mathbb{E}[\mathbf{x}_0|\mathbf{x}_t] - \mathbf{A}\mathbf{A}^T \lambda = \mathbf{0} \quad (49)$$

$$\Rightarrow \mathbf{A}\mathbf{A}^T \lambda = \mathbf{y} - \mathbf{A}\mathbb{E}[\mathbf{x}_0|\mathbf{x}_t] \quad (50)$$

Multiplying \mathbf{A}^\dagger to equation 50 and leveraging the property $\mathbf{A}^\dagger \mathbf{A}\mathbf{A}^T = \mathbf{A}^T$, we have

$$\mathbf{A}^T \lambda = \mathbf{A}^\dagger \mathbf{y} - \mathbf{A}^\dagger \mathbf{A}\mathbb{E}[\mathbf{x}_0|\mathbf{x}_t] \quad (51)$$

and consequently,

$$\hat{\mathbf{x}}_0 = \mathbb{E}[\mathbf{x}_0|\mathbf{x}_t] + \mathbf{A}^\dagger \mathbf{y} - \mathbf{A}^\dagger \mathbf{A}\mathbb{E}[\mathbf{x}_0|\mathbf{x}_t] \quad (52)$$

$$= \mathbf{A}^\dagger \mathbf{y} + (\mathbf{I} - \mathbf{A}^\dagger \mathbf{A})\mathbb{E}[\mathbf{x}_0|\mathbf{x}_t] \quad (53)$$

A.4. Proof of Theorem 4

We follow (Bao et al., 2022b) to derive the relationship between the optimal reverse variances $\mathbf{v}_t^2(\mathbf{x}_t)$ and optimal posterior variances $\mathbf{r}_t^2(\mathbf{x}_t)$ based on more general non-Markov forward process introduced by (Song et al., 2021a). To find the optimal solution to equation 19, we present a much simpler proof than (Bao et al., 2022b) using functional derivatives motivated by (Rezende & Viola, 2018). Given a noise schedule $\{\beta_t\}_{t=1}^T$ and $\alpha_t = 1 - \beta_t$, the forward process $q(\mathbf{x}_{1:T}|\mathbf{x}_0)$ is defined as

$$q(\mathbf{x}_{1:T}|\mathbf{x}_0) = q(\mathbf{x}_T|\mathbf{x}_0) \prod_{t=2}^T q(\mathbf{x}_{t-1}|\mathbf{x}_t, \mathbf{x}_0) \quad (54)$$

$$q(\mathbf{x}_{t-1}|\mathbf{x}_t, \mathbf{x}_0) = \mathcal{N}(\mathbf{x}_{t-1}|\tilde{\boldsymbol{\mu}}_t(\mathbf{x}_t, \mathbf{x}_0), \lambda_t^2 \mathbf{I}) \quad (55)$$

$$\tilde{\boldsymbol{\mu}}_t(\mathbf{x}_t, \mathbf{x}_0) = \sqrt{\bar{\alpha}_{t-1}}\mathbf{x}_0 + \sqrt{\bar{\beta}_{t-1} - \lambda_t^2} \cdot \frac{\mathbf{x}_t - \sqrt{\bar{\alpha}_t}\mathbf{x}_0}{\sqrt{\bar{\beta}_t}} \quad (56)$$

where $\bar{\alpha}_t = \prod_{i=1}^t \alpha_i$ and $\bar{\beta}_t = 1 - \bar{\alpha}_t$. (Song et al., 2021a) show that for arbitrary choice of λ_t , the marginal distributions $q(\mathbf{x}_t|\mathbf{x}_0)$ maintain $q(\mathbf{x}_t|\mathbf{x}_0) = \mathcal{N}(\mathbf{x}_t|\sqrt{\bar{\alpha}_t}\mathbf{x}_0, \bar{\beta}_t \mathbf{I})$. DDPM forward process is a special case when $\lambda_t^2 = \bar{\beta}_t$ with $\tilde{\beta}_t = \frac{\bar{\beta}_{t-1}}{\bar{\beta}_t} \beta_t$, which is used in (Nichol & Dhariwal, 2021) for pre-training DDPM model.

To fit the data distribution $q(\mathbf{x}_0)$, we define the reverse process, given by

$$p(\mathbf{x}_{0:T}) = p(\mathbf{x}_T) \prod_{t=1}^T p(\mathbf{x}_{t-1}|\mathbf{x}_t), \quad p(\mathbf{x}_{t-1}|\mathbf{x}_t) = \mathcal{N}(\mathbf{x}_{t-1}|\mathbf{m}_t(\mathbf{x}_t), \text{diag}[\mathbf{v}_t^2(\mathbf{x}_t)]) \quad (57)$$

To train $p(\mathbf{x}_0)$ we minimize the KL divergence between the forward and the reverse process:

$$\min_p D_{KL}(q(\mathbf{x}_{0:T})||p(\mathbf{x}_{0:T})), \quad q(\mathbf{x}_{0:T}) = q(\mathbf{x}_0)q(\mathbf{x}_{1:T}|\mathbf{x}_0) \quad (58)$$

which is equivalent to minimizing the variational bound $\mathbb{E}_q[L_{vb}]$ on negative log-likelihood of data distribution $q(\mathbf{x}_0)$ with L_{vb} given as follows:

$$L_{vb} = L_0 + L_1 + \dots + L_T \quad (59)$$

$$L_0 = -\log p(\mathbf{x}_0|\mathbf{x}_1) \quad (60)$$

$$L_{t-1} = D_{KL}(q(\mathbf{x}_{t-1}|\mathbf{x}_0, \mathbf{x}_t)||p(\mathbf{x}_{t-1}|\mathbf{x}_t)) \quad (61)$$

$$L_T = D_{KL}(q(\mathbf{x}_T|\mathbf{x}_0)||p(\mathbf{x}_T)) \quad (62)$$

For $t \in [2, T]$, L_{t-1} are KL divergences between two Gaussians, which possess analytical forms:

$$L_{t-1} \equiv \log \frac{|\text{diag}[\mathbf{v}_t^2(\mathbf{x}_t)]|}{|\lambda_t^2 \mathbf{I}|} + \|\tilde{\boldsymbol{\mu}}_t(\mathbf{x}_t, \mathbf{x}_0) - \mathbf{m}_t(\mathbf{x}_t)\|_{\text{diag}[\mathbf{v}_t^2(\mathbf{x}_t)]^{-1}}^2 + \text{tr}[\lambda_t^2 \text{diag}[\mathbf{v}_t^2(\mathbf{x}_t)]^{-1}] \quad (63)$$

$$\equiv \sum_{i=1}^d \log \mathbf{v}_t^2(\mathbf{x}_t)_i + \frac{(\tilde{\boldsymbol{\mu}}_t(\mathbf{x}_t, \mathbf{x}_0)_i - \mathbf{m}_t(\mathbf{x}_t)_i)^2}{\mathbf{v}_t^2(\mathbf{x}_t)_i} + \frac{\lambda_t^2}{\mathbf{v}_t^2(\mathbf{x}_t)_i} \quad (64)$$

where “ \equiv ” denotes “equals up to a constant and a scaling factor” and i indexes the elements of an vector.

Note that minimizing $\mathbb{E}_q[L_{vb}]$ can be decomposed into T independent optimization sub-problems:

$$\min_{\mathbf{m}_t, \mathbf{v}_t} \mathbb{E}_{q(\mathbf{x}_0, \mathbf{x}_t)}[L_{t-1}], \quad t \in [1, T] \quad (65)$$

The optimal \mathbf{m}_t and \mathbf{v}_t can be found by taking the functional derivatives of $\mathbb{E}_{q(\mathbf{x}_0, \mathbf{x}_t)}[L_{t-1}]$ w.r.t \mathbf{m}_t and \mathbf{v}_t^2 then set to zero:

$$\frac{\delta \mathbb{E}_{q(\mathbf{x}_0, \mathbf{x}_t)}[L_{t-1}]}{\delta \mathbf{m}_t(\mathbf{x}_t)_i} \equiv \mathbb{E}_{q(\mathbf{x}_0)}[q(\mathbf{x}_t|\mathbf{x}_0) \frac{\mathbf{m}_t(\mathbf{x}_t)_i - \tilde{\boldsymbol{\mu}}_t(\mathbf{x}_t, \mathbf{x}_0)_i}{\mathbf{v}_t^2(\mathbf{x}_t)_i}] = 0 \quad (66)$$

$$\frac{\delta \mathbb{E}_{q(\mathbf{x}_0, \mathbf{x}_t)}[L_{t-1}]}{\delta \mathbf{v}_t^2(\mathbf{x}_t)_i} \equiv \mathbb{E}_{q(\mathbf{x}_0)}[q(\mathbf{x}_t|\mathbf{x}_0) \left(\frac{1}{\mathbf{v}_t^2(\mathbf{x}_t)_i} - \frac{(\tilde{\boldsymbol{\mu}}_t(\mathbf{x}_t, \mathbf{x}_0)_i - \mathbf{m}_t(\mathbf{x}_t)_i)^2}{(\mathbf{v}_t^2(\mathbf{x}_t)_i)^2} - \frac{\lambda_t^2}{(\mathbf{v}_t^2(\mathbf{x}_t)_i)^2} \right)] = 0 \quad (67)$$

We can solve for optimal $\mathbf{m}_t(\mathbf{x}_t)_i$ by rearranging equation 66:

$$\mathbb{E}_{q(\mathbf{x}_0)}[q(\mathbf{x}_t|\mathbf{x}_0)]\mathbf{m}_t(\mathbf{x}_t)_i = \mathbb{E}_{q(\mathbf{x}_0)}[q(\mathbf{x}_t|\mathbf{x}_0)\tilde{\boldsymbol{\mu}}_t(\mathbf{x}_t, \mathbf{x}_0)_i] \quad (68)$$

$$\Rightarrow q(\mathbf{x}_t)\mathbf{m}_t(\mathbf{x}_t)_i = \int q(\mathbf{x}_0)q(\mathbf{x}_t|\mathbf{x}_0)\tilde{\boldsymbol{\mu}}_t(\mathbf{x}_t, \mathbf{x}_0)_i d\mathbf{x}_0 \quad (69)$$

$$\Rightarrow \mathbf{m}_t(\mathbf{x}_t)_i = \int q(\mathbf{x}_0|\mathbf{x}_t)\tilde{\boldsymbol{\mu}}_t(\mathbf{x}_t, \mathbf{x}_0)_i d\mathbf{x}_0 \quad (70)$$

$$\Rightarrow \mathbf{m}_t(\mathbf{x}_t)_i = \tilde{\boldsymbol{\mu}}_t(\mathbf{x}_t, \mathbb{E}[\mathbf{x}_0|\mathbf{x}_t])_i \quad (71)$$

where equation 71 is due to the linearity of $\tilde{\boldsymbol{\mu}}_t$ w.r.t \mathbf{x}_0 .

Likewise, rearranging equation 67 gives

$$\mathbf{v}_t^2(\mathbf{x}_t)_i = \lambda_t^2 + \mathbb{E}_{q(\mathbf{x}_0|\mathbf{x}_t)}[(\tilde{\boldsymbol{\mu}}_t(\mathbf{x}_t, \mathbf{x}_0)_i - \mathbf{m}_t(\mathbf{x}_t)_i)^2] \quad (72)$$

By plugging the optimal $\mathbf{m}_t(\mathbf{x}_t)_i$ determined by equation 71 into equation 72 and dropping the element index i , we conclude the proof:

$$\mathbf{v}_t^2(\mathbf{x}_t) = \lambda_t^2 + \mathbb{E}_{q(\mathbf{x}_0|\mathbf{x}_t)}[(\tilde{\boldsymbol{\mu}}_t(\mathbf{x}_t, \mathbf{x}_0) - \tilde{\boldsymbol{\mu}}_t(\mathbf{x}_t, \mathbb{E}[\mathbf{x}_0|\mathbf{x}_t]))^2] \quad (73)$$

$$= \lambda_t^2 + \mathbb{E}_{q(\mathbf{x}_0|\mathbf{x}_t)}[(\tilde{\boldsymbol{\mu}}_t(\mathbf{0}, \mathbf{x}_0 - \mathbb{E}[\mathbf{x}_0|\mathbf{x}_t]))^2] \quad (74)$$

$$= \lambda_t^2 + (\sqrt{\bar{\alpha}_{t-1}} - \sqrt{\bar{\beta}_{t-1}} - \lambda_t^2 \sqrt{\frac{\bar{\alpha}_t}{\bar{\beta}_t}})^2 \cdot \mathbb{E}_{q(\mathbf{x}_0|\mathbf{x}_t)}[(\mathbf{x}_0 - \mathbb{E}[\mathbf{x}_0|\mathbf{x}_t])^2] \quad (75)$$

$$= \lambda_t^2 + (\sqrt{\bar{\alpha}_{t-1}} - \sqrt{\bar{\beta}_{t-1}} - \lambda_t^2 \sqrt{\frac{\bar{\alpha}_t}{\bar{\beta}_t}})^2 \cdot \mathbf{r}_t^2(\mathbf{x}_t) \quad (76)$$

We are often given a pre-trained DDPM model with learned reverse variances. The following Corollary of Theorem 4 gives a simplified relationship between optimal posterior variances and optimal reverse variances under DDPM case:

Corollary 7. For the DDPM forward process $\lambda_t^2 = \tilde{\beta}_t$, the optimal posterior variances $\mathbf{r}_t^{*2}(\mathbf{x}_t)$ and optimal reverse variances $\mathbf{v}_t^{*2}(\mathbf{x}_t)$ are related by

$$\mathbf{v}_t^{*2}(\mathbf{x}_t) = \tilde{\beta}_t + \left(\frac{\sqrt{\bar{\alpha}_{t-1}}\beta_t}{1 - \bar{\alpha}_t}\right)^2 \cdot \mathbf{r}_t^{*2}(\mathbf{x}_t) \quad (77)$$

Remark 8. From Theorem 4, we also know that to perform optimal ancestral sampling, we only need to provide the MMSE estimator $\mathbb{E}[\mathbf{x}_0|\mathbf{x}_t]$ to compute the reverse mean $\mathbf{m}_t^*(\mathbf{x}_t)$ and the posterior variances $\mathbf{r}_t^{*2}(\mathbf{x}_t)$ to compute the reverse variances $\mathbf{v}_t^{*2}(\mathbf{x}_t)$, which can be both obtained from the proposed pre-training (equation 12). This may provide an alternative way for pre-training DDPM model that differs from (Nichol & Dhariwal, 2021).

A.5. Proof of Proposition 3

Deriving the optimal solution to equation 12 under the diagonal posterior covariance case, i.e., $\boldsymbol{\Sigma}_t(\mathbf{x}_t) = \text{diag}[\mathbf{r}_t^2(\mathbf{x}_t)]$, is similar to Appendix A.4. Note that we seek for point-wise maximizer of equation 12, i.e., find the optimum of

$$\mathbb{E}_{p_t(\mathbf{x}_0, \mathbf{x}_t)}[\log q_t(\mathbf{x}_0|\mathbf{x}_t)] \equiv \mathbb{E}_{p_t(\mathbf{x}_0, \mathbf{x}_t)}\left[\sum_{i=1}^d \frac{1}{\mathbf{r}_t^2(\mathbf{x}_t)_i} (\mathbf{x}_{0i} - \boldsymbol{\mu}_t(\mathbf{x}_t)_i)^2 + \log \mathbf{r}_t^2(\mathbf{x}_t)_i\right] \quad (78)$$

For any t , taking the functional derivatives of $\mathbb{E}_{p_t(\mathbf{x}_0, \mathbf{x}_t)}[\log q_t(\mathbf{x}_0|\mathbf{x}_t)]$ w.r.t $\boldsymbol{\mu}_t(\mathbf{x}_t)_i$ and $\mathbf{r}_t^2(\mathbf{x}_t)_i$ and then set to zero, we obtain the optimality conditions:

$$\mathbb{E}_{p(\mathbf{x}_0)}[p(\mathbf{x}_t|\mathbf{x}_0)(\boldsymbol{\mu}_t(\mathbf{x}_t)_i - \mathbf{x}_{0i})] = 0 \quad (79)$$

$$\mathbb{E}_{p(\mathbf{x}_0)}\left[p(\mathbf{x}_t|\mathbf{x}_0)\left(-\frac{1}{(\mathbf{r}_t^2(\mathbf{x}_t)_i)^2}(\mathbf{x}_{0i} - \boldsymbol{\mu}_t(\mathbf{x}_t)_i)^2 + \frac{1}{\mathbf{r}_t^2(\mathbf{x}_t)_i}\right)\right] = 0 \quad (80)$$

Combining the optimality conditions given by equation 79 and equation 80, we conclude the proof.

B. Closed-form Solutions for Implementing Guidances

In this section, we provide important closed-form results for implementing efficient Type I and Type II guidance under isotropic posterior covariance case: $\Sigma_t(\mathbf{x}_t) = r_t^2(\mathbf{x}_t)\mathbf{I}$. Before we delve into the closed-form results, we first give some important notations. We define the downsampling operator given sampling position $\mathbf{m} \in \{0, 1\}^{d \times 1}$ as $\mathbf{D}_{\mathbf{m}} \in \{0, 1\}^{\|\mathbf{m}\|_0 \times d}$, which selects rows of a given matrix that corresponds to one in \mathbf{m} and when performing left multiplication. We use $\mathbf{D}_{\downarrow s}$ to denote the standard s -folds downsampling operator, which is equivalent to $\mathbf{D}_{\mathbf{m}}$ when ones in \mathbf{m} are spaced evenly. For image signal, it selects the upper-left pixel for each distinct $s \times s$ patch (Zhang et al., 2020) when performing left multiplication to the *vectorized* image. We use $\mathbf{D}_{\downarrow s}$ to denote the distinct block downsampler, i.e., averaging s length d/s distinct blocks of a vector. For image signal, it averaging distinct $d/s \times d/s$ blocks (Zhang et al., 2020) when performing left multiplication to the *vectorized* image. We denote the Fourier transform matrix for d -dimensional signal as \mathbf{F} , Fourier transform matrix for d/s -dimensional signal as $\mathbf{F}_{\downarrow s}$, the Fourier transform of a vector \mathbf{v} as $\hat{\mathbf{v}}$, and the complex conjugate of a complex vector \mathbf{v} as $\bar{\mathbf{v}}$. We use \odot to denote element-wise multiplication, and the divisions used below are also element-wise.

Lemma 9. *Performing s -fold standard downsampling in spacial domain is equivalent to performing s -fold block downsampling in frequency domain: $\mathbf{D}_{\downarrow s} = \mathbf{F}_{\downarrow s} \mathbf{D}_{\downarrow s} \mathbf{F}^{-1}$.*

Proof. Considering an arbitrary d -dimensional signal in frequency domain $\hat{\mathbf{x}}[k]$, $k = 0, 2, \dots, d-1$. Multiplying $\mathbf{F}_{\downarrow s} \mathbf{D}_{\downarrow s} \mathbf{F}^{-1}$ to $\hat{\mathbf{x}}$ is equivalent to letting $\hat{\mathbf{x}}$ go through the following linear system and obtain the output $\hat{\mathbf{y}}$:

$$\mathbf{x}[n] = \frac{1}{d} \sum_{k=0}^{d-1} \hat{\mathbf{x}}[k] e^{j \frac{2\pi}{d} kn} \quad (81)$$

$$\mathbf{x}_{\downarrow s}[n] = \mathbf{x}[ns] \quad (82)$$

$$\hat{\mathbf{y}}[k] = \sum_{n=0}^{d/s-1} \mathbf{x}_{\downarrow s}[n] e^{-j \frac{2\pi}{d/s} kn} \quad (83)$$

We now use $\hat{\mathbf{x}}$ to represent $\hat{\mathbf{y}}$:

$$\hat{\mathbf{y}}[k] = \sum_{n=0}^{d/s-1} \frac{1}{d} \sum_{k'=0}^{d-1} \hat{\mathbf{x}}[k'] e^{j \frac{2\pi}{d} k' ns} e^{-j \frac{2\pi}{d/s} kn} \quad (84)$$

$$= \sum_{n=0}^{d/s-1} \frac{1}{d} e^{-j \frac{2\pi}{d/s} kn} \sum_{k'=0}^{d-1} \hat{\mathbf{x}}[k'] e^{j \frac{2\pi}{d/s} k' n} \quad (85)$$

$$= \sum_{n=0}^{d/s-1} \frac{1}{d} e^{-j \frac{2\pi}{d/s} kn} \left(\sum_{k'=0}^{d/s-1} + \sum_{k'=d/s}^{2d/s-1} + \sum_{k'=2d/s}^{3d/s-1} + \dots + \sum_{k'=(s-1)d/s}^{sd/s-1} \right) \hat{\mathbf{x}}[k'] e^{j \frac{2\pi}{d/s} k' n} \quad (86)$$

$$= \sum_{n=0}^{d/s-1} \frac{1}{d} e^{-j \frac{2\pi}{d/s} kn} \sum_{k'=0}^{d/s-1} (\hat{\mathbf{x}}[k'] + \hat{\mathbf{x}}[k' + d/s] + \dots + \hat{\mathbf{x}}[k' + (s-1)d/s]) e^{j \frac{2\pi}{d/s} k' n} \quad (87)$$

$$= \sum_{n=0}^{d/s-1} e^{-j \frac{2\pi}{d/s} kn} \frac{1}{d/s} \sum_{k'=0}^{d/s-1} \frac{\hat{\mathbf{x}}[k'] + \hat{\mathbf{x}}[k' + d/s] + \dots + \hat{\mathbf{x}}[k' + (s-1)d/s]}{s} e^{j \frac{2\pi}{d/s} k' n} \quad (88)$$

$$= \frac{\hat{\mathbf{x}}[k] + \hat{\mathbf{x}}[k + d/s] + \dots + \hat{\mathbf{x}}[k + (s-1)d/s]}{s} \quad (89)$$

where equation 87 is because $e^{j \frac{2\pi}{d/s} k' n}$ has period of d/s in k' and equation 89 is because d/s -dimensional inverse Fourier transform and Fourier transform are canceled out. From equation 89 we have $\hat{\mathbf{y}} = \mathbf{D}_{\downarrow s} \hat{\mathbf{x}}$. So $\mathbf{D}_{\downarrow s} \hat{\mathbf{x}} = \mathbf{F}_{\downarrow s} \mathbf{D}_{\downarrow s} \mathbf{F}^{-1} \hat{\mathbf{x}}$ for any $\hat{\mathbf{x}}$, and consequently, $\mathbf{D}_{\downarrow s} = \mathbf{F}_{\downarrow s} \mathbf{D}_{\downarrow s} \mathbf{F}^{-1}$. \square

B.1. Closed-form Solutions to Vector-Jacobian Products in Type I Guidance

When using Type I guidance, we are required to approximate the likelihood score, which can be approximated via vector-Jacobian product (Song et al., 2023):

$$\nabla_{\mathbf{x}_t} \log p(\mathbf{y}|\mathbf{x}_t) \approx (\mathbf{v}^T \frac{\partial \mathbb{E}[\mathbf{x}_0|\mathbf{x}_t]}{\partial \mathbf{x}_t})^T, \quad (90)$$

where $\mathbf{v} = \mathbf{A}^T(\sigma^2 \mathbf{I} + \mathbf{A}\Sigma_t(\mathbf{x}_t)\mathbf{A}^T)^{-1}(\mathbf{y} - \mathbf{A}\mathbb{E}[\mathbf{x}_0|\mathbf{x}_t])$. Below we provide closed-form solution to \mathbf{v} under three common degradation operators: i) inpainting, ii) deblurring, and iii) super resolution, then we can approximate the conditional posterior mean $\mathbb{E}[\mathbf{x}_0|\mathbf{x}_t, \mathbf{y}]$ based on proposition 1.

Inpainting. The observation model for image inpainting can be expressed as:

$$\mathbf{y} = \underbrace{\mathbf{D}_m}_{\mathbf{A}} \mathbf{x}_0 + \mathbf{n}, \quad (91)$$

and the closed-form solution to \mathbf{v} in image inpainting is given by the following:

$$\mathbf{v} = \frac{\tilde{\mathbf{y}} - \mathbf{m} \odot \mathbb{E}[\mathbf{x}_0|\mathbf{x}_t]}{\sigma^2 + r_t^2(\mathbf{x}_t)} \quad (92)$$

where $\tilde{\mathbf{y}} = \mathbf{D}_m^T \mathbf{y} = \mathbf{m} \odot (\mathbf{x}_0 + \tilde{\mathbf{n}})$, $\tilde{\mathbf{n}} \sim \mathcal{N}(\mathbf{0}, \mathbf{I})$ is the zero-filling measurements that fills the masked region with zeros and processes the exact same size to \mathbf{x}_0 . In practice, the measurements in inpainting are usually stored in the form of $\tilde{\mathbf{y}}$, while \mathbf{y} used here is for mathematical convenient.

Proof.

$$\mathbf{v} = \mathbf{D}_m^T (\sigma^2 \mathbf{I} + \mathbf{D}_m r_t^2(\mathbf{x}_t) \mathbf{I} \mathbf{D}_m^T)^{-1} (\mathbf{y} - \mathbf{D}_m \mathbb{E}[\mathbf{x}_0|\mathbf{x}_t]) \quad (93)$$

$$= \mathbf{D}_m^T (\sigma^2 \mathbf{I} + r_t^2(\mathbf{x}_t) \mathbf{D}_m \mathbf{D}_m^T)^{-1} (\mathbf{y} - \mathbf{D}_m \mathbb{E}[\mathbf{x}_0|\mathbf{x}_t]) \quad (94)$$

$$= \mathbf{D}_m^T ((\sigma^2 + r_t^2(\mathbf{x}_t)) \mathbf{I})^{-1} (\mathbf{y} - \mathbf{D}_m \mathbb{E}[\mathbf{x}_0|\mathbf{x}_t]) \quad (95)$$

$$= \frac{\mathbf{D}_m^T (\mathbf{y} - \mathbf{D}_m \mathbb{E}[\mathbf{x}_0|\mathbf{x}_t])}{\sigma^2 + r_t^2(\mathbf{x}_t)} \quad (96)$$

$$= \frac{\tilde{\mathbf{y}} - \mathbf{m} \odot \mathbb{E}[\mathbf{x}_0|\mathbf{x}_t]}{\sigma^2 + r_t^2(\mathbf{x}_t)} \quad (97)$$

where equation 95 and equation 97 are because $\mathbf{D}_m \mathbf{D}_m^T = \mathbf{I}$ and $\mathbf{D}_m^T \mathbf{D}_m = \text{diag}[\mathbf{m}]$. \square

Deblurring. The observation model for image deblurring can be expressed as:

$$\mathbf{y} = \mathbf{x}_0 * \mathbf{k} + \mathbf{n}, \quad (98)$$

where \mathbf{k} is the blurring kernel and $*$ is convolution operator. By assuming $*$ is a circular convolution operator, we can convert equation 98 to the canonical form $\mathbf{y} = \mathbf{A}\mathbf{x}_0 + \mathbf{n}$ by leveraging the convolution property of Fourier transform:

$$\mathbf{y} = \underbrace{\mathbf{F}^{-1} \text{diag}[\hat{\mathbf{k}}] \mathbf{F}}_{\mathbf{A}} \mathbf{x}_0 + \mathbf{n}, \quad (99)$$

and the closed-form solution to \mathbf{v} in image deblurring is given by the following:

$$\mathbf{v} = \mathbf{F}^{-1} (\tilde{\hat{\mathbf{k}}} \odot \frac{\mathbf{F}(\mathbf{y} - \mathbf{A}\mathbb{E}[\mathbf{x}_0|\mathbf{x}_t])}{\sigma^2 + r_t^2(\mathbf{x}_t) \tilde{\hat{\mathbf{k}}} \odot \hat{\mathbf{k}}}). \quad (100)$$

Proof. Since \mathbf{A} is a real matrix, we have $\mathbf{A}^T = \mathbf{A}^H = \mathbf{F}^{-1} \text{diag}[\tilde{\mathbf{k}}] \mathbf{F}$, then

$$\mathbf{v} = \mathbf{F}^{-1} \text{diag}[\tilde{\mathbf{k}}] \mathbf{F} (\sigma^2 \mathbf{I} + \mathbf{F}^{-1} \text{diag}[\hat{\mathbf{k}}] \mathbf{F} r_t^2(\mathbf{x}_t) \mathbf{I} \mathbf{F}^{-1} \text{diag}[\tilde{\mathbf{k}}] \mathbf{F})^{-1} (\mathbf{y} - \mathbf{A} \mathbb{E}[\mathbf{x}_0 | \mathbf{x}_t]) \quad (101)$$

$$= \mathbf{F}^{-1} \text{diag}[\tilde{\mathbf{k}}] \mathbf{F} (\sigma^2 \mathbf{I} + r_t^2(\mathbf{x}_t) \mathbf{F}^{-1} \text{diag}[\hat{\mathbf{k}}] \text{diag}[\tilde{\mathbf{k}}] \mathbf{F})^{-1} (\mathbf{y} - \mathbf{A} \mathbb{E}[\mathbf{x}_0 | \mathbf{x}_t]) \quad (102)$$

$$= \mathbf{F}^{-1} \text{diag}[\tilde{\mathbf{k}}] \mathbf{F} (\sigma^2 \mathbf{I} + r_t^2(\mathbf{x}_t) \mathbf{F}^{-1} \text{diag}[\hat{\mathbf{k}} \odot \tilde{\mathbf{k}}] \mathbf{F})^{-1} (\mathbf{y} - \mathbf{A} \mathbb{E}[\mathbf{x}_0 | \mathbf{x}_t]) \quad (103)$$

$$= \mathbf{F}^{-1} \text{diag}[\tilde{\mathbf{k}}] \mathbf{F} (\mathbf{F}^{-1} (\sigma^2 \mathbf{I} + r_t^2(\mathbf{x}_t) \text{diag}[\hat{\mathbf{k}} \odot \tilde{\mathbf{k}}]) \mathbf{F})^{-1} (\mathbf{y} - \mathbf{A} \mathbb{E}[\mathbf{x}_0 | \mathbf{x}_t]) \quad (104)$$

$$= \mathbf{F}^{-1} \text{diag}[\tilde{\mathbf{k}}] \mathbf{F} (\mathbf{F}^{-1} \text{diag}[\sigma^2 + r_t^2(\mathbf{x}_t) \hat{\mathbf{k}} \odot \tilde{\mathbf{k}}] \mathbf{F})^{-1} (\mathbf{y} - \mathbf{A} \mathbb{E}[\mathbf{x}_0 | \mathbf{x}_t]) \quad (105)$$

$$= \mathbf{F}^{-1} \text{diag}[\tilde{\mathbf{k}}] \mathbf{F} \mathbf{F}^{-1} \text{diag}[\sigma^2 + r_t^2(\mathbf{x}_t) \hat{\mathbf{k}} \odot \tilde{\mathbf{k}}]^{-1} \mathbf{F} (\mathbf{y} - \mathbf{A} \mathbb{E}[\mathbf{x}_0 | \mathbf{x}_t]) \quad (106)$$

$$= \mathbf{F}^{-1} (\tilde{\mathbf{k}} \odot \frac{\mathbf{F} (\mathbf{y} - \mathbf{A} \mathbb{E}[\mathbf{x}_0 | \mathbf{x}_t])}{\sigma^2 + r_t^2(\mathbf{x}_t) \hat{\mathbf{k}} \odot \tilde{\mathbf{k}}}) \quad (107)$$

□

Super resolution. According to (Zhang et al., 2020), the observation model for image super resolution can be *approximately* expressed as:

$$\mathbf{y} = (\mathbf{x}_0 * \mathbf{k})_{\downarrow s} + \mathbf{n} \quad (108)$$

By leveraging the convolution property of Fourier transform, we can convert equation 108 to the canonical form $\mathbf{y} = \mathbf{A} \mathbf{x}_0 + \mathbf{n}$:

$$\mathbf{y} = \underbrace{\mathbf{D}_{\downarrow s} \mathbf{F}^{-1} \text{diag}[\hat{\mathbf{k}}] \mathbf{F}}_{\mathbf{A}} \mathbf{x}_0 + \mathbf{n} \quad (109)$$

and the closed-form solution to \mathbf{v} in image super resolution is given by the following:

$$\mathbf{v} = \mathbf{F}^{-1} (\tilde{\mathbf{k}} \odot_s \frac{\mathbf{F}_{\downarrow s} (\mathbf{y} - \mathbf{A} \mathbb{E}[\mathbf{x}_0 | \mathbf{x}_t])}{\sigma^2 + r_t^2(\mathbf{x}_t) (\tilde{\mathbf{k}} \odot \hat{\mathbf{k}})_{\downarrow s}}) \quad (110)$$

where \odot_s denotes block processing operator with element-wise multiplication (Zhang et al., 2020).

Proof. Since \mathbf{A} is a real matrix, we have $\mathbf{A}^T = \mathbf{A}^H = \mathbf{F}^{-1} \text{diag}[\tilde{\mathbf{k}}] \mathbf{F} \mathbf{D}_{\downarrow s}^T$, then

$$\mathbf{v} = \mathbf{F}^{-1} \text{diag}[\tilde{\mathbf{k}}] \mathbf{F} \mathbf{D}_{\downarrow s}^T (\sigma^2 \mathbf{I} + \mathbf{D}_{\downarrow s} \mathbf{F}^{-1} \text{diag}[\hat{\mathbf{k}}] \mathbf{F} r_t^2(\mathbf{x}_t) \mathbf{I} \mathbf{F}^{-1} \text{diag}[\tilde{\mathbf{k}}] \mathbf{F} \mathbf{D}_{\downarrow s}^T)^{-1} (\mathbf{y} - \mathbf{A} \mathbb{E}[\mathbf{x}_0 | \mathbf{x}_t]) \quad (111)$$

$$= \mathbf{F}^{-1} \text{diag}[\tilde{\mathbf{k}}] \mathbf{F} \mathbf{D}_{\downarrow s}^T (\sigma^2 \mathbf{I} + r_t^2(\mathbf{x}_t) \mathbf{D}_{\downarrow s} \mathbf{F}^{-1} \text{diag}[\hat{\mathbf{k}} \odot \tilde{\mathbf{k}}] \mathbf{F} \mathbf{D}_{\downarrow s}^T)^{-1} (\mathbf{y} - \mathbf{A} \mathbb{E}[\mathbf{x}_0 | \mathbf{x}_t]) \quad (112)$$

$$= \mathbf{F}^{-1} \text{diag}[\tilde{\mathbf{k}}] \mathbf{F} \mathbf{D}_{\downarrow s}^T (\mathbf{D}_{\downarrow s} \mathbf{F}^{-1} (\sigma^2 \mathbf{I} + r_t^2(\mathbf{x}_t) \text{diag}[\hat{\mathbf{k}} \odot \tilde{\mathbf{k}}]) \mathbf{F} \mathbf{D}_{\downarrow s}^T)^{-1} (\mathbf{y} - \mathbf{A} \mathbb{E}[\mathbf{x}_0 | \mathbf{x}_t]) \quad (113)$$

$$= \mathbf{F}^{-1} \text{diag}[\tilde{\mathbf{k}}] \mathbf{F} \mathbf{D}_{\downarrow s}^T (\mathbf{D}_{\downarrow s} \mathbf{F}^{-1} \text{diag}[\sigma^2 + r_t^2(\mathbf{x}_t) \hat{\mathbf{k}} \odot \tilde{\mathbf{k}}] \mathbf{F} \mathbf{D}_{\downarrow s}^T)^{-1} (\mathbf{y} - \mathbf{A} \mathbb{E}[\mathbf{x}_0 | \mathbf{x}_t]) \quad (114)$$

By Lemma 9, we have $\mathbf{D}_{\downarrow s} \mathbf{F}^{-1} = \mathbf{F}_{\downarrow s}^{-1} \mathbf{D}_{\downarrow s}$. Taking the hermitian transpose to both side and leveraging $\mathbf{F}^{-1} = \frac{1}{d} \mathbf{F}^H$ and $\mathbf{F}_{\downarrow s}^{-1} = \frac{1}{d/s} \mathbf{F}_{\downarrow s}^H$, we also have $\mathbf{F} \mathbf{D}_{\downarrow s}^T = s \mathbf{D}_{\downarrow s}^T \mathbf{F}_{\downarrow s}$. So

$$\mathbf{v} = \mathbf{F}^{-1} \text{diag}[\tilde{\mathbf{k}}] s \mathbf{D}_{\downarrow s}^T \mathbf{F}_{\downarrow s} (\mathbf{F}_{\downarrow s}^{-1} \mathbf{D}_{\downarrow s} \text{diag}[\sigma^2 + r_t^2(\mathbf{x}_t) \hat{\mathbf{k}} \odot \tilde{\mathbf{k}}] s \mathbf{D}_{\downarrow s}^T \mathbf{F}_{\downarrow s})^{-1} (\mathbf{y} - \mathbf{A} \mathbb{E}[\mathbf{x}_0 | \mathbf{x}_t]) \quad (115)$$

$$= \mathbf{F}^{-1} \text{diag}[\tilde{\mathbf{k}}] s \mathbf{D}_{\downarrow s}^T \mathbf{F}_{\downarrow s} (\mathbf{F}_{\downarrow s}^{-1} \text{diag}[\sigma^2 + r_t^2(\mathbf{x}_t) (\hat{\mathbf{k}} \odot \tilde{\mathbf{k}})_{\downarrow s}] \mathbf{F}_{\downarrow s})^{-1} (\mathbf{y} - \mathbf{A} \mathbb{E}[\mathbf{x}_0 | \mathbf{x}_t]) \quad (116)$$

$$= \mathbf{F}^{-1} \text{diag}[\tilde{\mathbf{k}}] s \mathbf{D}_{\downarrow s}^T \mathbf{F}_{\downarrow s} \mathbf{F}_{\downarrow s}^{-1} \text{diag}[\sigma^2 + r_t^2(\mathbf{x}_t) (\hat{\mathbf{k}} \odot \tilde{\mathbf{k}})_{\downarrow s}]^{-1} \mathbf{F}_{\downarrow s} (\mathbf{y} - \mathbf{A} \mathbb{E}[\mathbf{x}_0 | \mathbf{x}_t]) \quad (117)$$

$$= \mathbf{F}^{-1} (\tilde{\mathbf{k}} \odot_s \mathbf{D}_{\downarrow s}^T \frac{\mathbf{F}_{\downarrow s} (\mathbf{y} - \mathbf{A} \mathbb{E}[\mathbf{x}_0 | \mathbf{x}_t])}{\sigma^2 + r_t^2(\mathbf{x}_t) (\hat{\mathbf{k}} \odot \tilde{\mathbf{k}})_{\downarrow s}}) \quad (118)$$

$$= \mathbf{F}^{-1} (\tilde{\mathbf{k}} \odot_s \frac{\mathbf{F}_{\downarrow s} (\mathbf{y} - \mathbf{A} \mathbb{E}[\mathbf{x}_0 | \mathbf{x}_t])}{\sigma^2 + r_t^2(\mathbf{x}_t) (\hat{\mathbf{k}} \odot \tilde{\mathbf{k}})_{\downarrow s}}) \quad (119)$$

□

B.2. Closed-form Solutions to Proximal Problems in Type II Guidance

When using Type II guidance, we are required to solve the following *auto-weighted* proximal problem:

$$\mathbb{E}_q[\mathbf{x}_0|\mathbf{x}_t, \mathbf{y}] = \arg \min_{\mathbf{x}_0} \|\mathbf{y} - \mathbf{A}\mathbf{x}_0\|^2 + \sigma^2 \|\mathbf{x}_0 - \mathbb{E}[\mathbf{x}_0|\mathbf{x}_t]\|_{\Sigma_t^{-1}(\mathbf{x}_t)}^2 \quad (120)$$

which has general closed-form solution given by

$$\mathbb{E}_q[\mathbf{x}_0|\mathbf{x}_t, \mathbf{y}] = (\Sigma_t(\mathbf{x}_t)^{-1} + \frac{1}{\sigma^2} \mathbf{A}^T \mathbf{A})^{-1} (\Sigma_t(\mathbf{x}_t)^{-1} \mathbb{E}[\mathbf{x}_0|\mathbf{x}_t] + \frac{1}{\sigma^2} \mathbf{A}^T \mathbf{y}) \quad (121)$$

The derivation of equation 121 can be directly obtained via computing the mean of $q_t(\mathbf{x}_0|\mathbf{x}_t, \mathbf{y})$ by using the Bayes' theorem for Gaussian variables (Bishop, 2006).

Below we provide closed-form solution to $\mathbb{E}_q[\mathbf{x}_0|\mathbf{x}_t, \mathbf{y}]$ under three common degradation operators same as for Type I guidance, then we can directly replace the denoising result in unconditional diffusion step with the closed-form solution of $\mathbb{E}_q[\mathbf{x}_0|\mathbf{x}_t, \mathbf{y}]$ to solve target inverse problem. The closed-form results are obtained by borrowing the results from (Zhu et al., 2023) and setting ρ_t to $\frac{\sigma^2}{r_t^2(\mathbf{x}_t)}$.

Inpainting. The observation model for image inpainting see equation 91, and the closed-form solution to $\mathbb{E}_q[\mathbf{x}_0|\mathbf{x}_t, \mathbf{y}]$ is given as follows:

$$\mathbb{E}_q[\mathbf{x}_0|\mathbf{x}_t, \mathbf{y}] = \frac{\tilde{\mathbf{y}} + \rho_t \mathbb{E}[\mathbf{x}_0|\mathbf{x}_t]}{\rho_t + \mathbf{m}}, \quad \rho_t = \frac{\sigma^2}{r_t^2(\mathbf{x}_t)} \quad (122)$$

Deblurring. The observation model for image deblurring see equation 98 and equation 99, and the closed-form solution to $\mathbb{E}_q[\mathbf{x}_0|\mathbf{x}_t, \mathbf{y}]$ is given as follows:

$$\mathbb{E}_q[\mathbf{x}_0|\mathbf{x}_t, \mathbf{y}] = \mathbf{F}^{-1} \frac{\tilde{\mathbf{k}} \odot \mathbf{F}\mathbf{y} + \rho_t \mathbf{F}\mathbb{E}[\mathbf{x}_0|\mathbf{x}_t]}{\tilde{\mathbf{k}} \odot \hat{\mathbf{k}} + \rho_t}, \quad \rho_t = \frac{\sigma^2}{r_t^2(\mathbf{x}_t)} \quad (123)$$

Super resolution. The observation model for image super resolution see equation 108 and equation 109, and the closed-form solution to $\mathbb{E}_q[\mathbf{x}_0|\mathbf{x}_t, \mathbf{y}]$ is given as follows:

$$\mathbb{E}_q[\mathbf{x}_0|\mathbf{x}_t, \mathbf{y}] = \mathbf{F}^{-1} \frac{1}{\rho_t} \left(\mathbf{d} - \tilde{\mathbf{k}} \odot_s \frac{(\hat{\mathbf{k}} \odot \mathbf{d})_{\downarrow_s}}{(\tilde{\mathbf{k}} \odot \hat{\mathbf{k}})_{\downarrow_s} + \rho_t} \right), \quad \rho_t = \frac{\sigma^2}{r_t^2(\mathbf{x}_t)} \quad (124)$$

where $\mathbf{d} = \hat{\mathbf{k}} \odot (\mathbf{F}\mathbf{y}_{\uparrow_s}) + \rho_t \mathbf{F}\mathbb{E}[\mathbf{x}_0|\mathbf{x}_t]$ and \uparrow_s denotes the standard s -fold upsampling, i.e., upsampling the spatial size by filling the new entries with zeros (Zhang et al., 2020).

C. Using Conjugate Gradient Method for General Posterior Covariance

For general posterior covariance, the closed-form solution for \mathbf{v} or $\mathbb{E}_q[\mathbf{x}_0|\mathbf{x}_t, \mathbf{y}]$ is usually unavailable. However, we can still approximate their solutions by using numerical solutions of linear equations. Specifically, we can see that for Type II guidance, $\mathbb{E}_q[\mathbf{x}_0|\mathbf{x}_t, \mathbf{y}]$ satisfies the following linear equation:

$$(\Sigma_t(\mathbf{x}_t)^{-1} + \frac{1}{\sigma^2} \mathbf{A}^T \mathbf{A}) \mathbb{E}_q[\mathbf{x}_0|\mathbf{x}_t, \mathbf{y}] = \Sigma_t(\mathbf{x}_t)^{-1} \mathbb{E}[\mathbf{x}_0|\mathbf{x}_t] + \frac{1}{\sigma^2} \mathbf{A}^T \mathbf{y} \quad (125)$$

Since $\Sigma_t(\mathbf{x}_t)^{-1} + \frac{1}{\sigma^2} \mathbf{A}^T \mathbf{A}$ is in fact the precision matrix of $q_t(\mathbf{x}_0|\mathbf{x}_t, \mathbf{y})$, we know that it is symmetric and positive-definite. Therefore, we can solve equation 125 using conjugate gradient (CG) method (Hestenes et al., 1952).

Likewise, for Type I guidance, it easy to see that $\sigma^2 \mathbf{I} + \mathbf{A}\Sigma_t(\mathbf{x}_t)\mathbf{A}^T$ is symmetric and positive-definite. To approximate \mathbf{v} , we define a temporal variable \mathbf{u} , and approximate it using CG to solve the following linear equation:

$$(\sigma^2 \mathbf{I} + \mathbf{A}\Sigma_t(\mathbf{x}_t)\mathbf{A}^T) \mathbf{u} = \mathbf{y} - \mathbf{A}\mathbb{E}[\mathbf{x}_0|\mathbf{x}_t] \quad (126)$$

Then \mathbf{v} can be obtained as follows:

$$\mathbf{v} = \mathbf{A}^T \mathbf{u} \quad (127)$$

In our experiments, only the Convert-type posterior covariance (Section 4.1) requires to use the CG method, as the posterior covariances used in prior works and Analytic-type posterior covariance (Section 4.2) are isotropic that possess closed-form solutions. We use the black box CG method implemented in `scipy.sparse.linalg.cg` with `tol=1e-4`.

D. Additional Experimental Details and Results

D.1. Additional Quantitative Results

In this section, we report the FID (Figure 5) and SSIM (Figure 6) performance for supplementary results of Type II guidance.

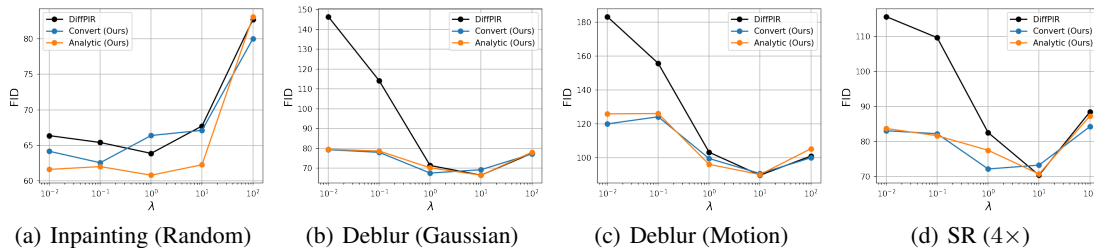


Figure 5: **Quantitative results (FID) on FFHQ dataset for Type II guidance.** We report the FID performance under different λ .

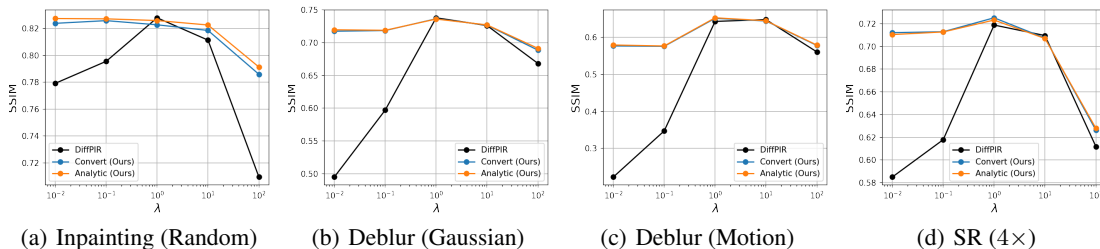


Figure 6: **Quantitative results (SSIM) on FFHQ dataset for Type II guidance.** We report the SSIM performance under different λ .

D.2. Converting Optimal Solutions Between Different Perturbation Kernels

Suppose we are given a family of optimal solutions q_t defined by the following MLE objectives for all $t \in [0, T]$:

$$\max_{q_t} \mathbb{E}_{\mathbf{x}_0 \sim p(\mathbf{x}_0), \epsilon \sim \mathcal{N}(\mathbf{0}, \mathbf{I})} \log q_t(\mathbf{x}_0 | \mathbf{x}_t = s_t(\mathbf{x}_0 + \sigma_t \epsilon)) \quad (128)$$

As can be seen, q_t equals the optimal solutions to equation 12 when the perturbation kernels $p_t(\mathbf{x}_t | \mathbf{x}_0)$ are set to $\mathcal{N}(\mathbf{x}_t | s_t \mathbf{x}_0, s_t^2 \sigma_t^2 \mathbf{I})$. Now, suppose we want to perform sampling based on the diffusion ODE (SDE) under the perturbation kernels $\mathcal{N}(\mathbf{x}_t | \tilde{s}_t \mathbf{x}_0, \tilde{s}_t^2 \tilde{\sigma}_t^2 \mathbf{I})$. This means that we are required to provide optimal solutions \tilde{q}_t defined by the following objectives for all $t \in [0, T]$:

$$\max_{\tilde{q}_t} \mathbb{E}_{\mathbf{x}_0 \sim p(\mathbf{x}_0), \epsilon \sim \mathcal{N}(\mathbf{0}, \mathbf{I})} \log \tilde{q}_t(\mathbf{x}_0 | \mathbf{x}_t = \tilde{s}_t(\mathbf{x}_0 + \tilde{\sigma}_t \epsilon)) \quad (129)$$

The idea is that, \tilde{q}_t can be directly represented by q_t , so we do not require to perform re-training:

$$\tilde{q}_t(\mathbf{x}_0 | \mathbf{x}_t = \mathbf{x}) = q_{t'}(\mathbf{x}_0 | \mathbf{x}_{t'} = \frac{s_{t'}}{\tilde{s}_t} \mathbf{x}), \quad \sigma_{t'} = \tilde{\sigma}_t \quad (130)$$

Proof. We only need to show that \tilde{q}_t defined by equation 128 and equation 130 are equivalent to \tilde{q}_t defined by equation 129. From equation 130, we actually know that $q_{t'}(\mathbf{x}_0|\mathbf{x}_{t'} = \mathbf{x}) = \tilde{q}_t(\mathbf{x}_0|\mathbf{x}_t = \frac{\tilde{s}_t}{s_{t'}}\mathbf{x})$, plug it in equation 128 at t' we have

$$\max_{\tilde{q}_t} \mathbb{E}_{\mathbf{x}_0 \sim p(\mathbf{x}_0), \epsilon \sim \mathcal{N}(\mathbf{0}, \mathbf{I})} \log \tilde{q}_t(\mathbf{x}_0|\mathbf{x}_t = \tilde{s}_t(\mathbf{x}_0 + \sigma_{t'}\epsilon)), \quad \sigma_{t'} = \tilde{\sigma}_t \quad (131)$$

which is equivalent to equation 129. \square

For example, suppose we are given optimal solutions q_t under DDPM perturbation kernels, i.e., $p_t(\mathbf{x}_t|\mathbf{x}_0) = \mathcal{N}(\mathbf{x}_t|\sqrt{\alpha_t}\mathbf{x}_0, \tilde{\beta}_t\mathbf{I})$. We aim to convert these solutions to optimal solutions \tilde{q}_t under perturbation kernels used in Section 2.2, i.e., $p_t(\mathbf{x}_t|\mathbf{x}_0) = \mathcal{N}(\mathbf{x}_t|\mathbf{x}_0, t^2\mathbf{I})$. We can realize it using following two steps: (1) finding t' such that $\sqrt{\frac{\tilde{\beta}_{t'}}{\alpha_{t'}}} = t$, and (2) scaling the input of $q_{t'}$ by the factor of $\sqrt{\alpha_{t'}}$. Formally,

$$\tilde{q}_t(\mathbf{x}_0|\mathbf{x}_t = \mathbf{x}) = q_{t'}(\mathbf{x}_0|\mathbf{x}_{t'} = \sqrt{\alpha_{t'}}\mathbf{x}), \quad \sqrt{\frac{\tilde{\beta}_{t'}}{\alpha_{t'}}} = t \quad (132)$$

D.3. Implementation of DDNM Solutions

Using DDNM solution (equation 11) for Type II guidance in noiseless inverse problems requires to compute the pseudo-inverse \mathbf{A}^\dagger for a given linear operator \mathbf{A} . Below we present the implementations of the pseudo-inverses used in our experiments.

Inpainting. We construct the DDNM solution $\mathbb{E}_q[\mathbf{x}_0|\mathbf{x}_t, \mathbf{y}]$ for the inpainting case $\mathbf{A} = \mathbf{D}_m$ as follows

$$\mathbb{E}_q[\mathbf{x}_0|\mathbf{x}_t, \mathbf{y}] = \tilde{\mathbf{y}} + (1 - \mathbf{m}) \odot \mathbb{E}[\mathbf{x}_0|\mathbf{x}_t] \quad (133)$$

Proof. Since $\mathbf{D}_m\mathbf{D}_m^T = \mathbf{I}$ is non-singular, we can directly obtain \mathbf{A}^\dagger by $\mathbf{A}^\dagger = \mathbf{D}_m^T(\mathbf{D}_m\mathbf{D}_m^T)^{-1} = \mathbf{D}_m^T$. Plug in equation 11, we have

$$\mathbb{E}_q[\mathbf{x}_0|\mathbf{x}_t, \mathbf{y}] = \mathbf{D}_m^T\mathbf{y} + (\mathbf{I} - \mathbf{D}_m^T\mathbf{D}_m)\mathbb{E}[\mathbf{x}_0|\mathbf{x}_t] \quad (134)$$

$$= \tilde{\mathbf{y}} + (\mathbf{I} - \text{diag}[\mathbf{m}])\mathbb{E}[\mathbf{x}_0|\mathbf{x}_t] \quad (135)$$

$$= \tilde{\mathbf{y}} + \text{diag}[1 - \mathbf{m}]\mathbb{E}[\mathbf{x}_0|\mathbf{x}_t] \quad (136)$$

$$= \tilde{\mathbf{y}} + (1 - \mathbf{m}) \odot \mathbb{E}[\mathbf{x}_0|\mathbf{x}_t] \quad (137)$$

\square

Deblurring. We construct the pseudo inverse \mathbf{A}^\dagger for the linear operator in the deblurring case $\mathbf{A} = \mathbf{F}^{-1}\text{diag}[\hat{\mathbf{k}}]\mathbf{F}$ as follows

$$\mathbf{A}^\dagger = \mathbf{F}^{-1}\text{diag}[\hat{\mathbf{k}}]^\dagger\mathbf{F} \quad (138)$$

where $\text{diag}[\hat{\mathbf{k}}]^\dagger$ is defined as $\text{diag}[\hat{\mathbf{k}}]^\dagger = \text{diag}[[l_1, l_2, \dots]^T]$ with $l_i = 0$ if $\hat{\mathbf{k}}_i = 0$ ⁸ otherwise $l_i = 1/\hat{\mathbf{k}}_i$.

Proof. It is easy to see that with the above construction, \mathbf{A}^\dagger satisfies $\mathbf{A}\mathbf{A}^\dagger\mathbf{A} = \mathbf{A}$. \square

Super resolution. We directly use `torch.nn.functional.interpolate` in place of \mathbf{A}^\dagger for the super resolution case.

D.4. Inference Time Analysis

The speed of inference of our method depends on whether `Analytic` or `Convert` is chosen.

In the case of `Analytic`, our method does not impose any additional computational cost for online inference compared to previous works. The computational expense arises from the offline pre-calculation of \hat{r}_t^2 using equation 24. Similar to (Bao et al., 2022b), a small number of Monte Carlo samples is typically adequate for obtaining an accurate \hat{r}_t . With a pre-trained

⁸Numerically, $|\hat{\mathbf{k}}_i|$ is always larger than zero. We threshold $\hat{\mathbf{k}}_i$ to zero when $|\hat{\mathbf{k}}_i| < 3 \times 10^{-2}$ similar to (Wang et al., 2023)

unconditional model and training dataset, we compute \hat{r}_t offline and deploy it alongside the pre-trained unconditional model. As a result, the online inference cost of our method is the same as previous methods. In our paper, we initially calculate \hat{r}_t using a randomly selected 0.5% of the training set and reuse it for all our experiments. This process takes a couple of hours on a single 1080Ti GPU.

For `Convert`, the CG method can introduce additional computational cost. However, we’ve observed that CG converges rapidly (~ 5 steps when initialize at $D_t(\mathbf{x}_t) \approx \mathbb{E}[\mathbf{x}_0|\mathbf{x}_t]$) and is only employed during the last few sampling steps. The additional computational cost of CG is negligible compared to the overall inference time.

D.5. Correlation Reduction Using Orthonormal Transform

The main drawback of current plug-and-play posterior covariance optimization methods is the oversimplified diagonal covariance structure, which assumes pixels are uncorrelated. If we are allowed to train unconditional diffusion models from scratch, we may wish to model the pixel correlation for potential performance enhancement. In this section, we present a scalable way for modeling correlation using orthonormal transform (OT), which is motivated by transform coding (TC) in image compression literature (Ballé et al., 2020). Specifically, we assume \mathbf{x}_0 is represented by some orthonormal basis Ψ , such that

$$\mathbf{x}_0 = \Psi\theta_0 \tag{139}$$

By the property of covariance, we have

$$\text{Cov}[\mathbf{x}_0|\mathbf{x}_t] = \Psi\text{Cov}[\theta_0|\mathbf{x}_t]\Psi^T \tag{140}$$

Assume the elements of θ_0 are mutually independent. Since given condition \mathbf{x}_t is equivalent to given θ_0 plus isotropic Gaussian noise, the elements of $\theta_0|\mathbf{x}_t$ are also mutually independent. This motivates that, if the elements of θ_0 are more “closed to” mutually independent than \mathbf{x}_0 using proper basis, $\text{Cov}[\theta_0|\mathbf{x}_t]$ could be better approximated by a diagonal matrix than $\text{Cov}[\mathbf{x}_0|\mathbf{x}_t]$. Thereby, we parameterize the covariance of the variational Gaussian posterior $q_t(\mathbf{x}_0|\mathbf{x}_t)$ as

$$\Sigma_t(\mathbf{x}_t) = \Psi\text{diag}[\mathbf{r}_t^2(\mathbf{x}_t)]\Psi^T \tag{141}$$

The main benefit of using orthonormal basis for parameterizing $\Sigma_t(\mathbf{x}_t)$ is that the number of values to predict in $\Sigma_t(\mathbf{x}_t)$ is reduced from d^2 to d , which can be a significant reduction for image data ($d > 10^5$), and the training procedure can be simply implemented as learning diagonal Gaussian posterior in the transform space (latent space).

Guidance	Method	Inpaint (Random)			Deblur (Gaussian)			Deblur (Motion)			Super resolution (4x)		
		SSIM \uparrow	LPIPS \downarrow	FID \downarrow	SSIM \uparrow	LPIPS \downarrow	FID \downarrow	SSIM \uparrow	LPIPS \downarrow	FID \downarrow	SSIM \uparrow	LPIPS \downarrow	FID \downarrow
I	DCTVar (Ours)	0.9067	0.1128	40.42	0.7824	0.2077	66.80	0.7499	0.2407	78.23	0.7827	0.2171	70.24
	SpatialVar (Ours)	0.9271	0.0931	34.43	0.7872	0.2026	64.78	0.7513	0.2392	78.49	0.7835	0.2171	70.68
	PIGDM	0.8759	0.1651	59.84	0.7844	0.2107	68.62	0.7497	0.2436	76.28	0.7793	0.2204	71.43
II	DCTVar (Ours)	0.8952	0.1160	37.93	0.7428	0.2290	79.05	0.6786	0.2876	108.74	0.7345	0.2473	92.89
	SpatialVar (Ours)	0.8446	0.1658	60.91	0.7299	0.2352	78.94	0.6405	0.3132	121.20	0.7165	0.2579	91.44
	PIGDM	0.8597	0.1603	58.94	0.7340	0.2383	82.25	0.6377	0.3245	130.83	0.7124	0.2662	100.94

Table 5: **Results for covariance with OT on FFHQ dataset.** We use **red** when there is no improvement over baseline.

We pretrain unconditional diffusion models based on k-diffusion code base for predicting three values: 1) posterior mean $\mathbb{E}[\mathbf{x}_0|\mathbf{x}_t]$, 2) $\mathbf{r}_t^2(\mathbf{x}_t)$ when Ψ is set to identity matrix, referred to as spatial variance, and 3) $\mathbf{r}_t^2(\mathbf{x}_t)$ when Ψ is set to DCT basis, referred to as DCT variance. Example model predictions see Figure 7. To compare different posterior covariance for solving inverse problems, similar to Section 5.2, the optimal posterior covariance is used only at the low noise level (For spatial variance, $\sigma_t < 0.2$; For DCT variance, $\sigma_t < 1$), while for high noise level, we use IIGDM covariance.

Table 5 presents the evaluation results for different covariances. IIGDM is IIGDM posterior covariance discussed in Section 3.1. DCTVar and SpatialVar are posterior covariance parameterized using Ψ set to DCT basis and identity matrix respectively (equation 140). We observed that, a notable improvement with DCTVar is its performance under high noise levels. Unlike SpatialVar, which performs poorly under high noise levels and is only used when $\sigma_t < 0.2$, DCTVar can be used for significantly higher noise levels, and even for all sampling steps without hurting the performance. This is because a Gaussian with DCTVar fits the posterior more closely under high noise levels, while a Gaussian with SpatialVar can only be effective under lower noise levels.

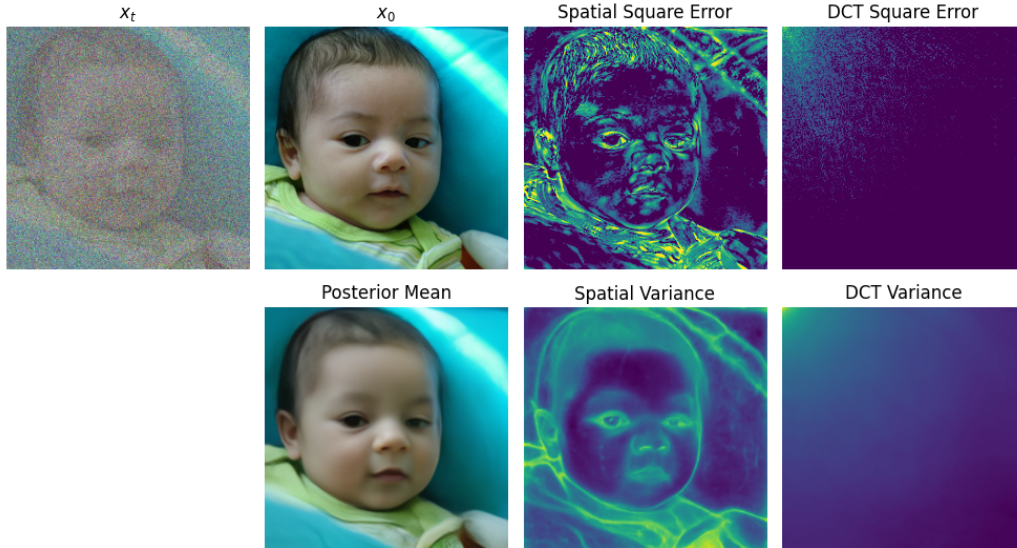


Figure 7: **Ground truths and model predictions.** σ_t is set to 1; Spatial Square Error refers to $(x_0 - \mathbb{E}[x_0|x_t])^2$, and DCT Square Error refers to $(\Psi^T x_0 - \Psi^T \mathbb{E}[x_0|x_t])^2$, where Ψ is DCT basis; As can be seen, Spatial Square Error and DCT Square Error can be predicted by Spatial Variance and DCT Variance, respectively.

D.6. Qualitative Results

In this section, we present additional visual examples using FFHQ datasets to showcase the capabilities of our method. Figure 8, 9, 10, and 11 serve as complementary visual examples to Table 3. These illustrations consistently demonstrate that our optimal covariances generate superior images compared to previous heuristic covariances in Type I guidance. Furthermore, Figure 12 demonstrates how our methods can enhance the robustness of DiffPIR against the hyper-parameter λ , taking random inpainting as an example. We also display the notable performance improvement of IIGDM with the adaptive weight, i.e., complete version of IIGDM, in Figure 13, 14, 15, and 16. Lastly, Figure 17 illustrates that our methods can enhance the DPS robustness to the hyper-parameter ζ , using random inpainting as an example.

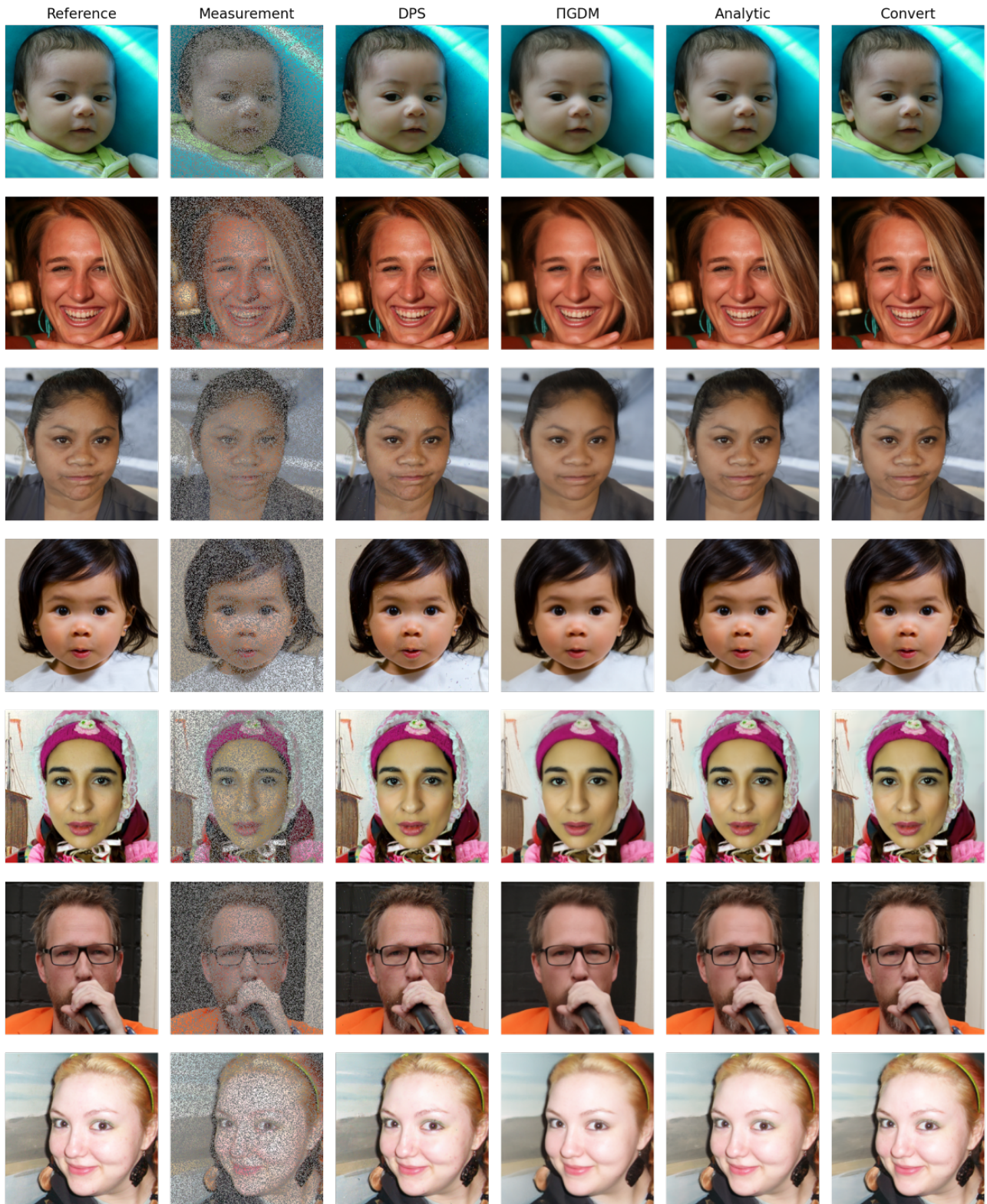


Figure 8: Qualitative results for Table 3 on random inpainting.

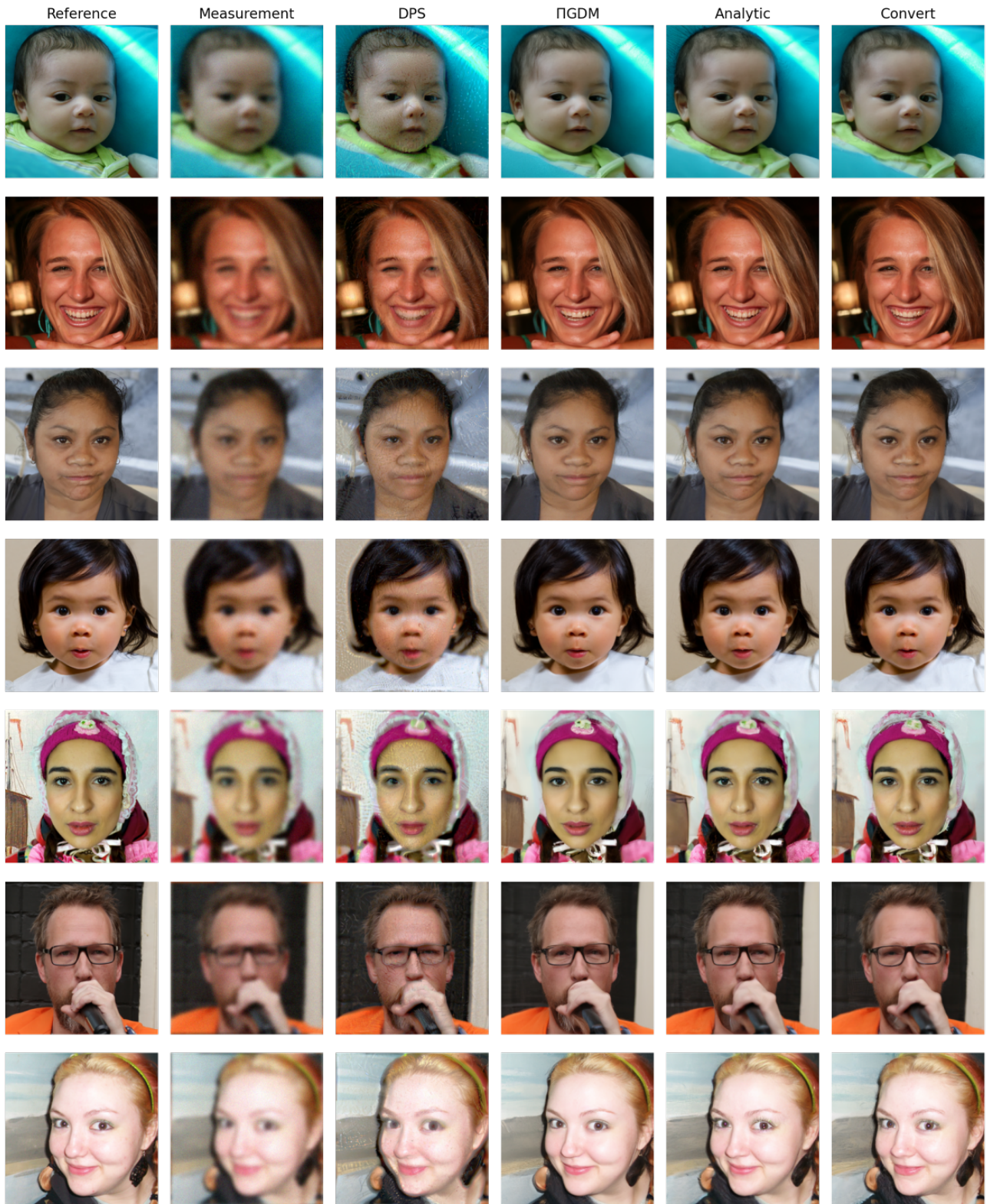


Figure 9: Qualitative results for Table 3 on Gaussian deblurring.

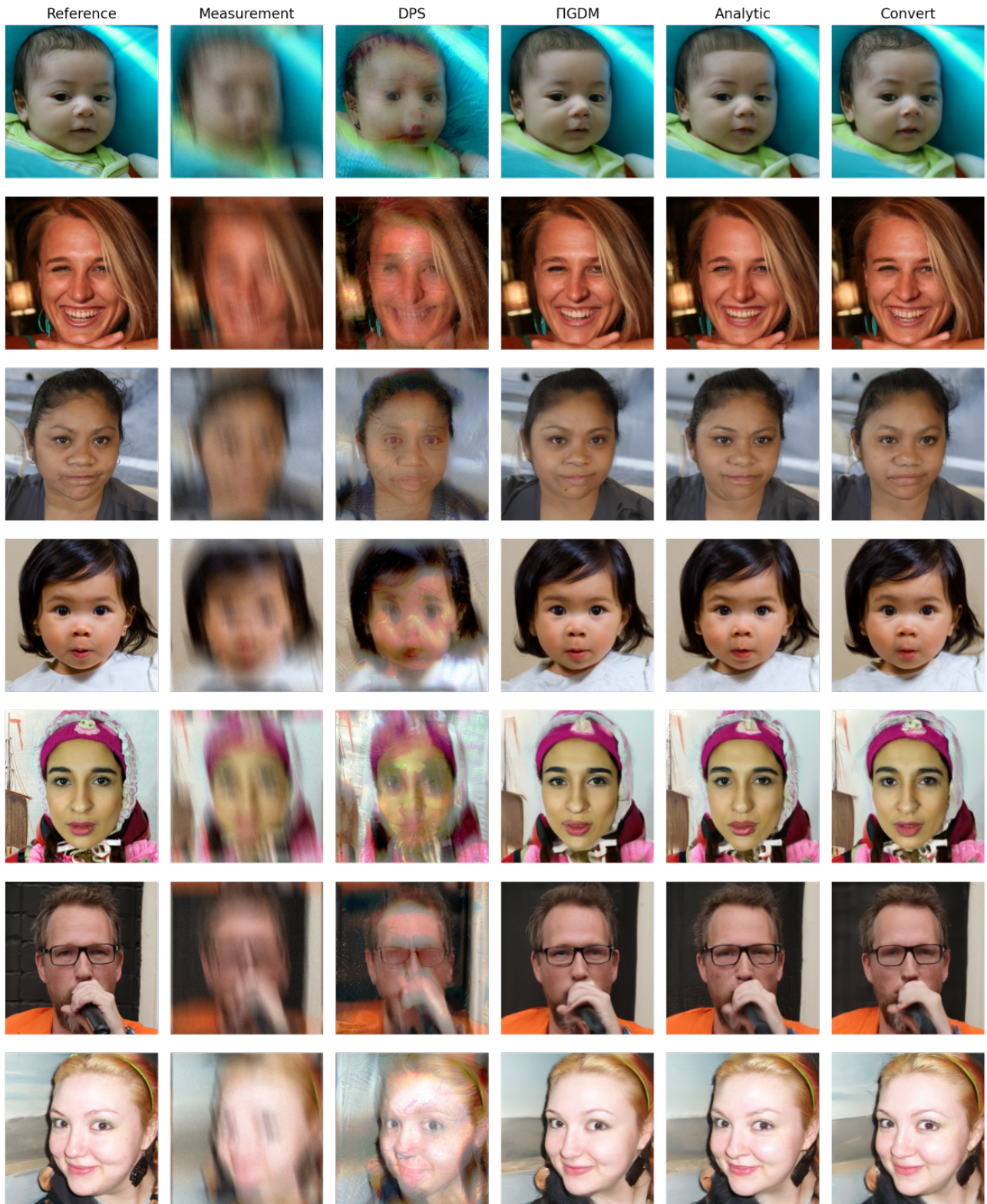


Figure 10: Qualitative results for Table 3 on motion deblurring.

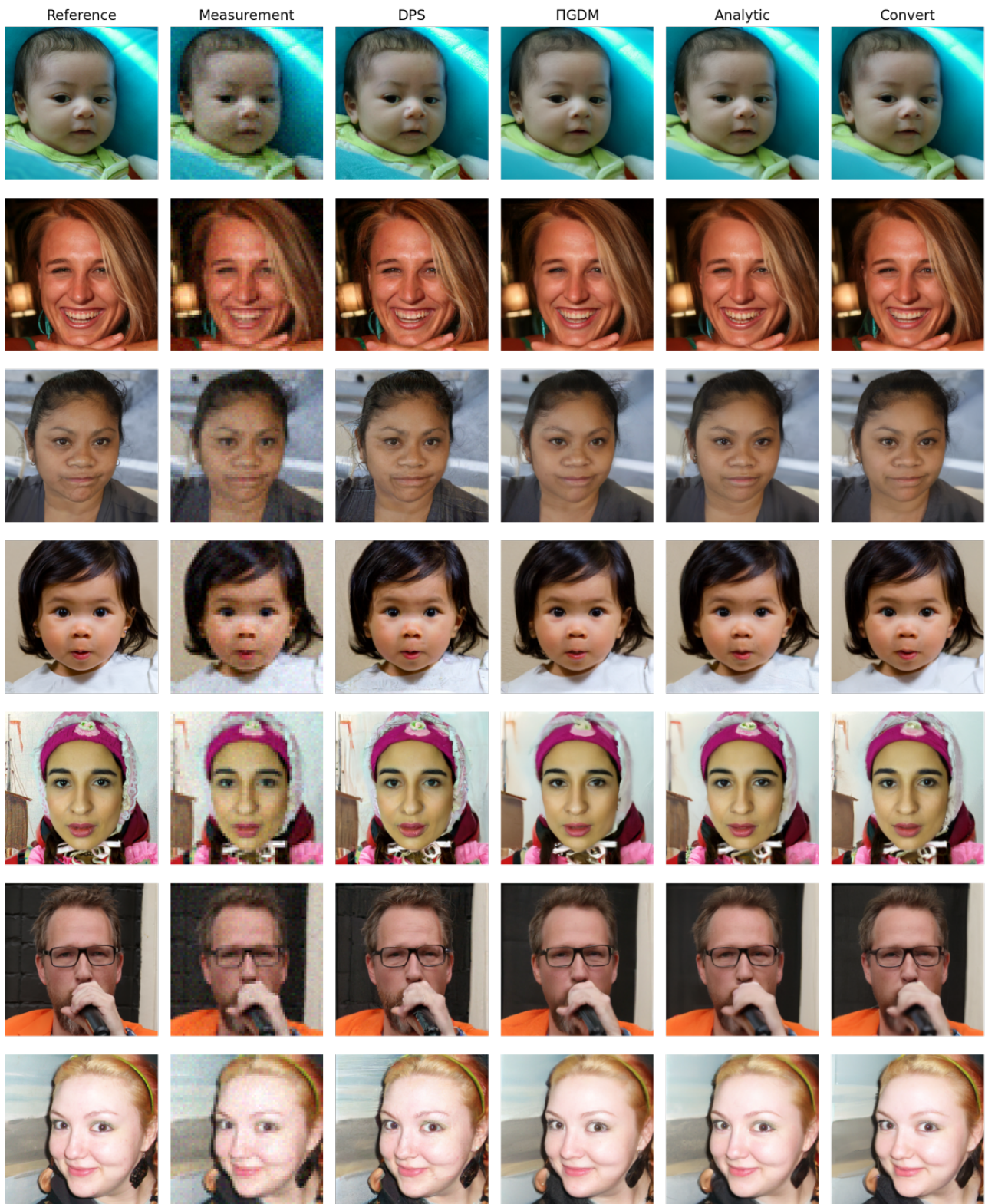
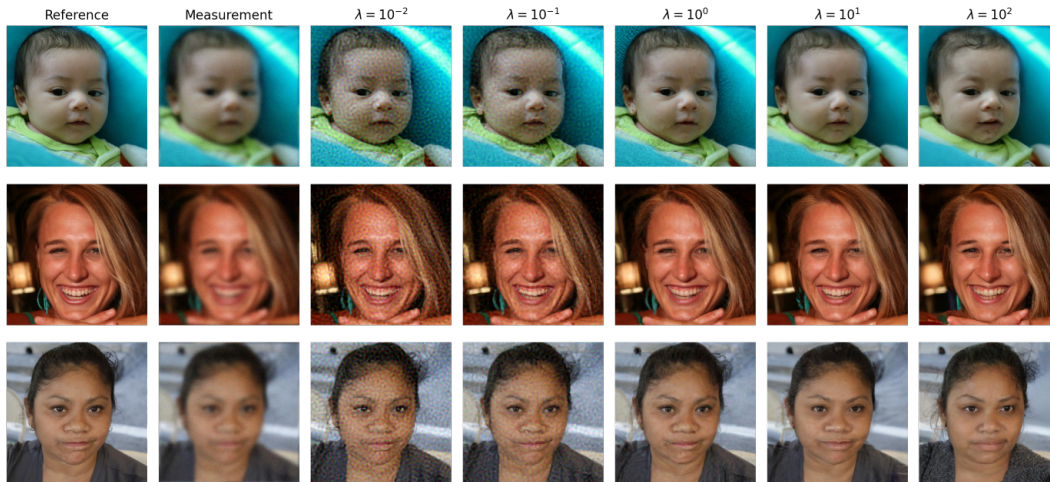
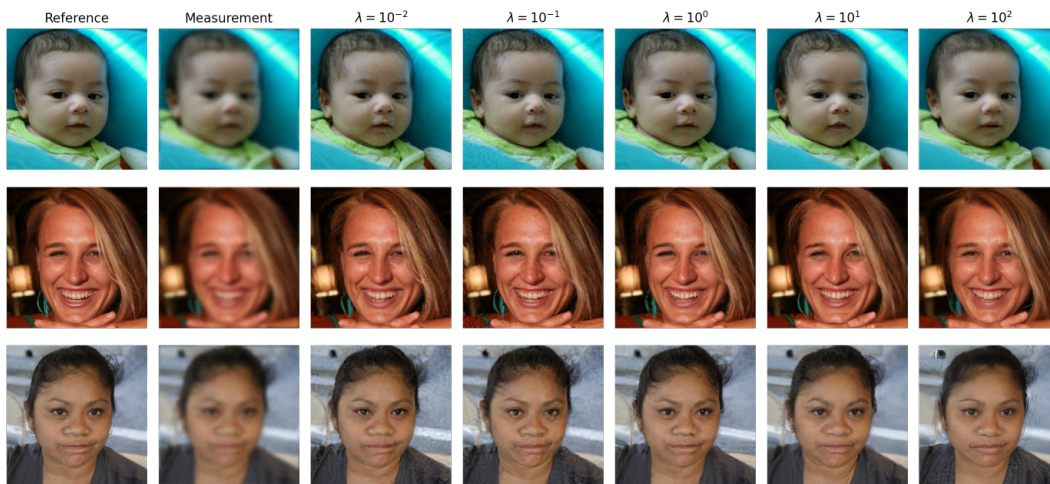


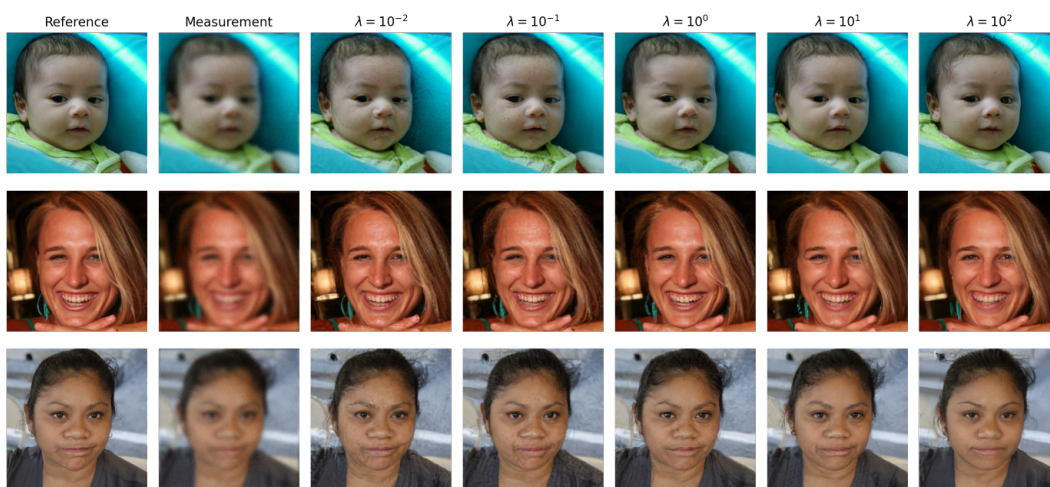
Figure 11: Qualitative results for Table 3 on super resolution (4 \times).



(a) DiffPIR



(b) Analytic



(c) Convert

Figure 12: **Qualitative results for Type II guidance on Gaussian deblurring under different λ .** As can be seen, our methods significantly improve DiffPIR robustness to the hyper-parameter λ .

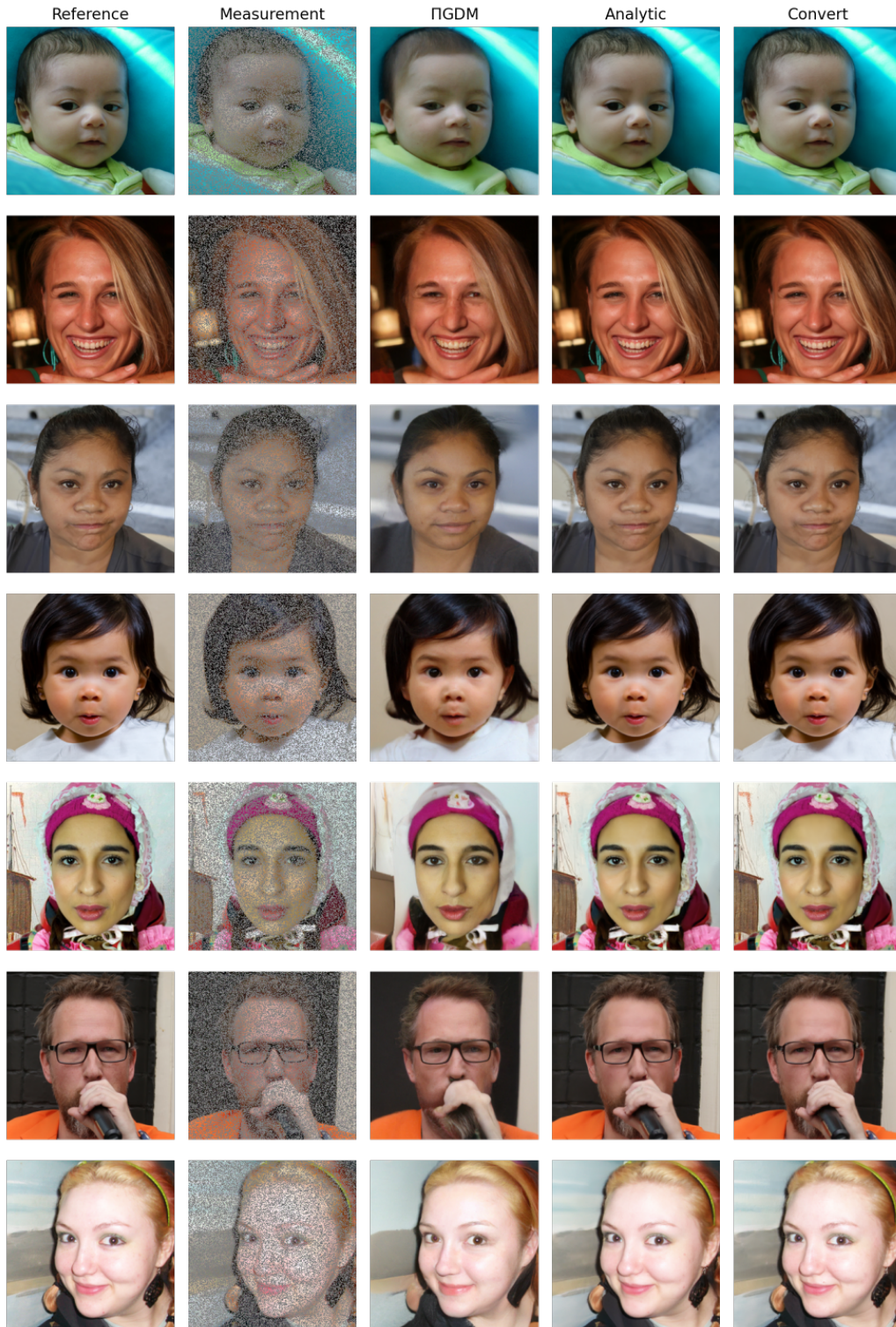


Figure 13: Qualitative results for complete Π GDM on random inpainting.

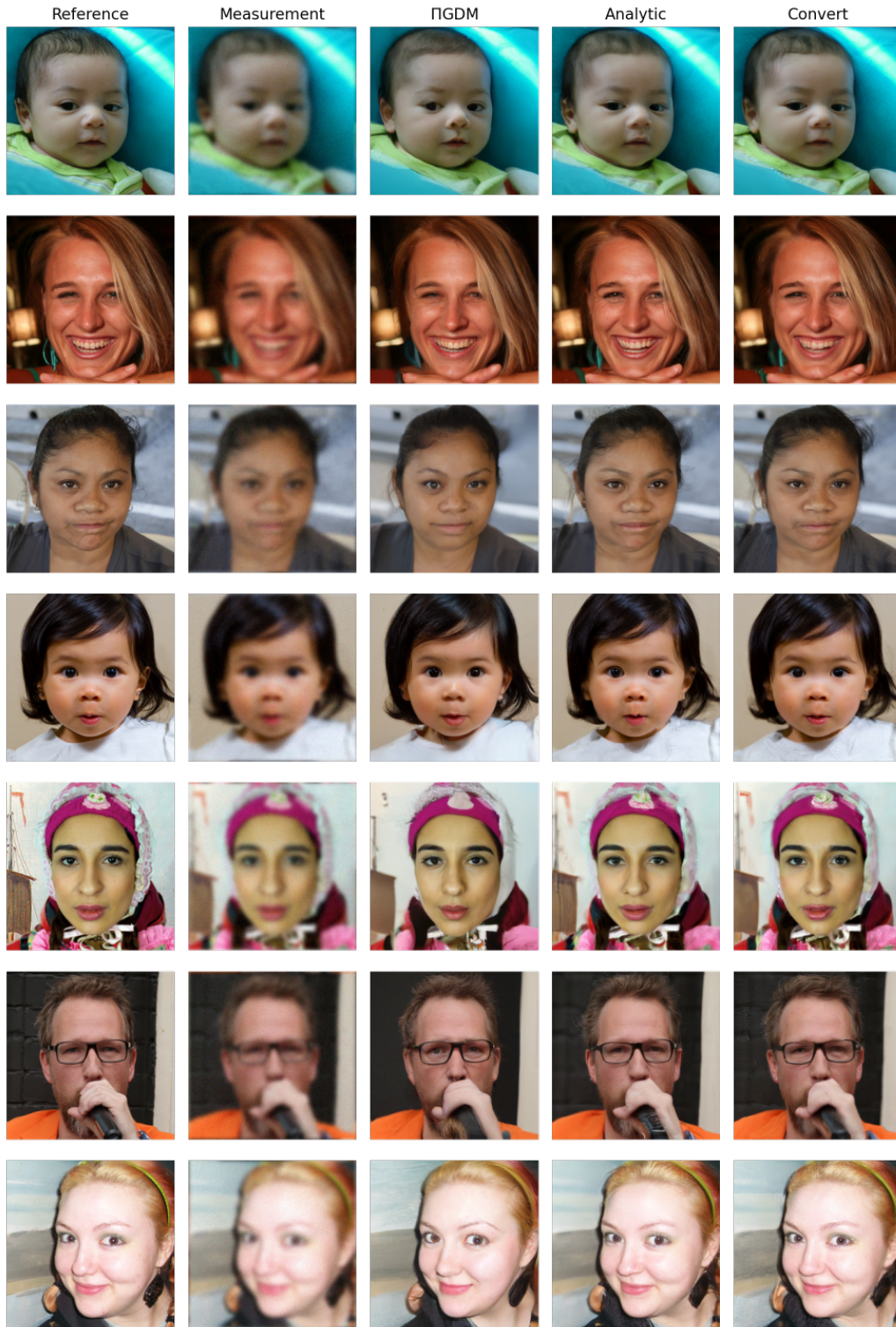


Figure 14: Qualitative results for complete Π GDM on Gaussian deblurring.

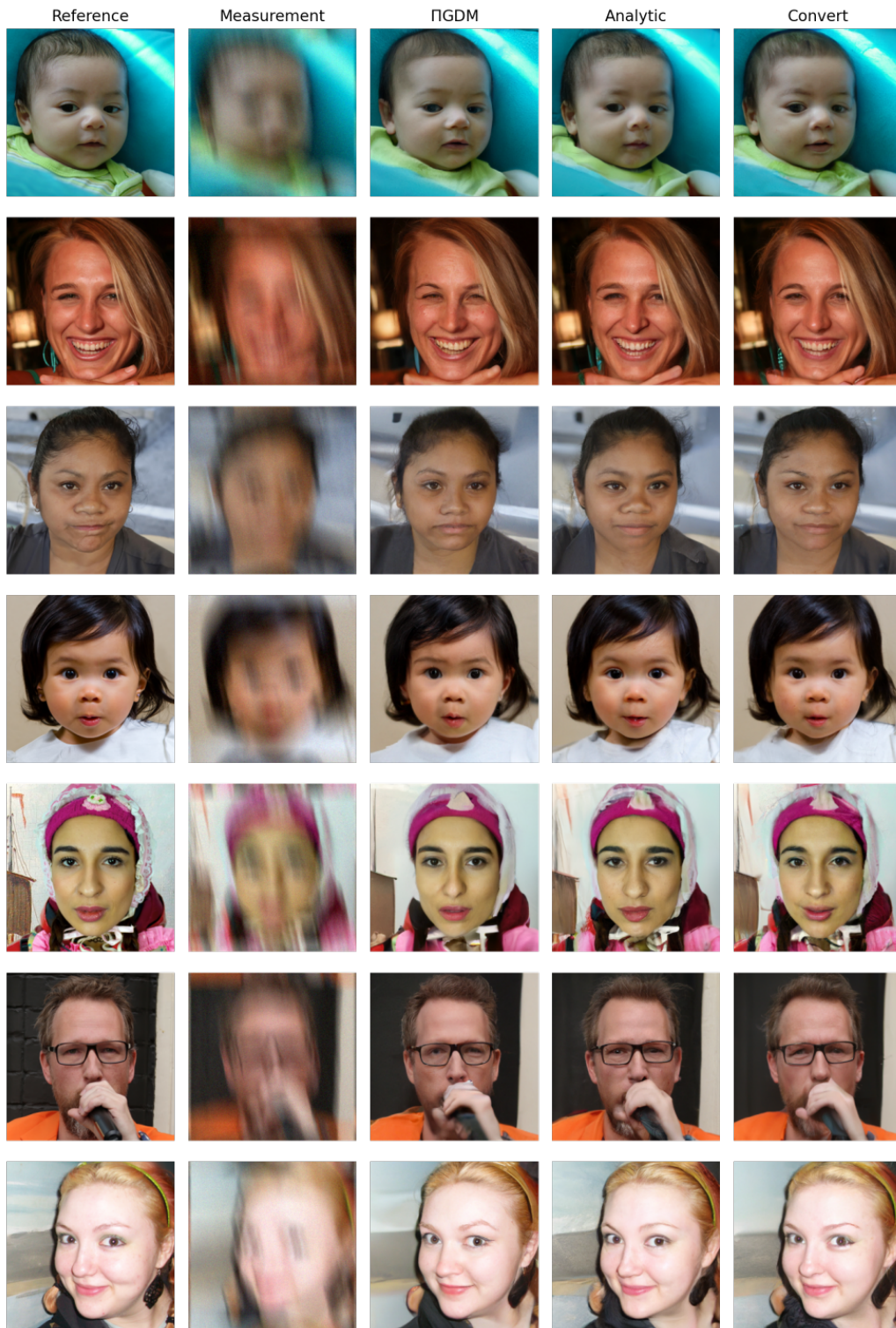


Figure 15: Qualitative results for complete Π GDM on motion deblurring.

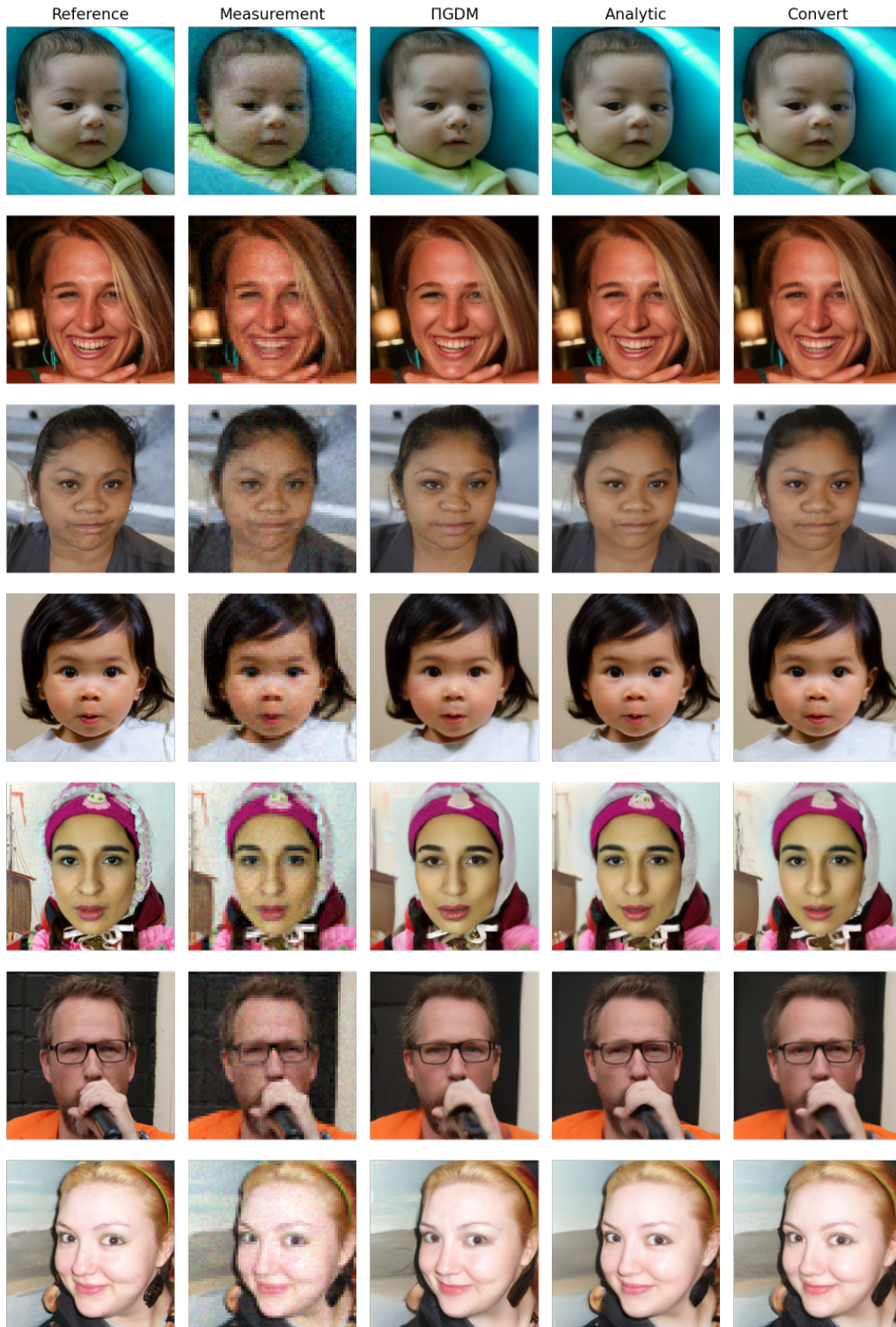
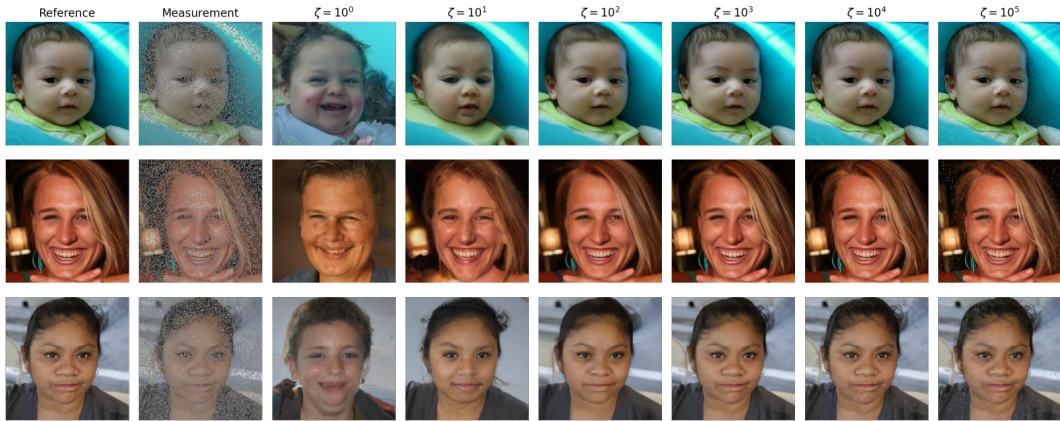
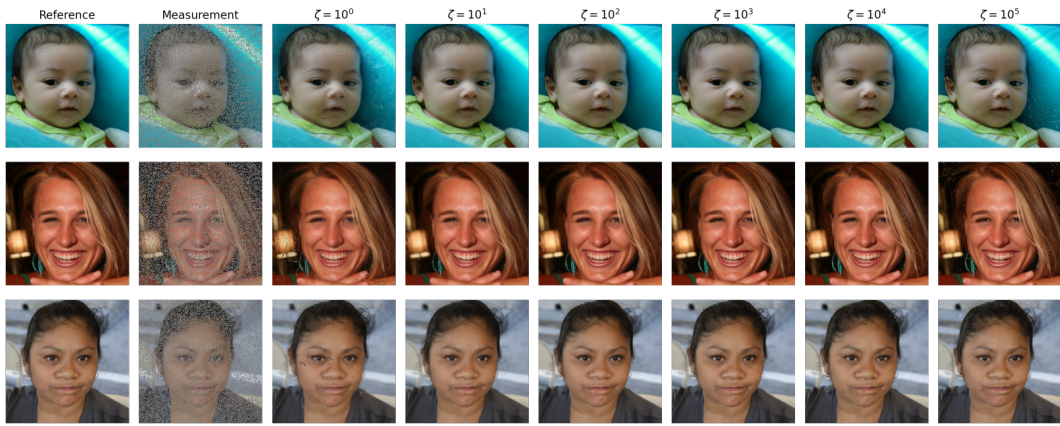


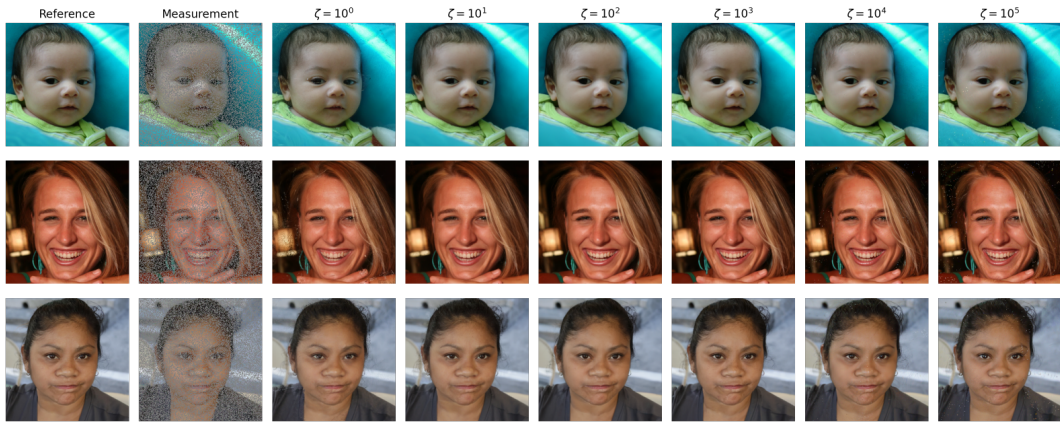
Figure 16: Qualitative results for complete Π GDM on super resolution ($4\times$).



(a) DPS



(b) Analytic



(c) Convert

Figure 17: **Qualitative results for complete version of DPS on random inpainting.** As can be seen, our methods significantly improve DPS robustness to the hyper-parameter ζ .